Cell

Recessive epistasis of a synonymous mutation confers cucumber domestication through epitranscriptomic regulation

Graphical abstract

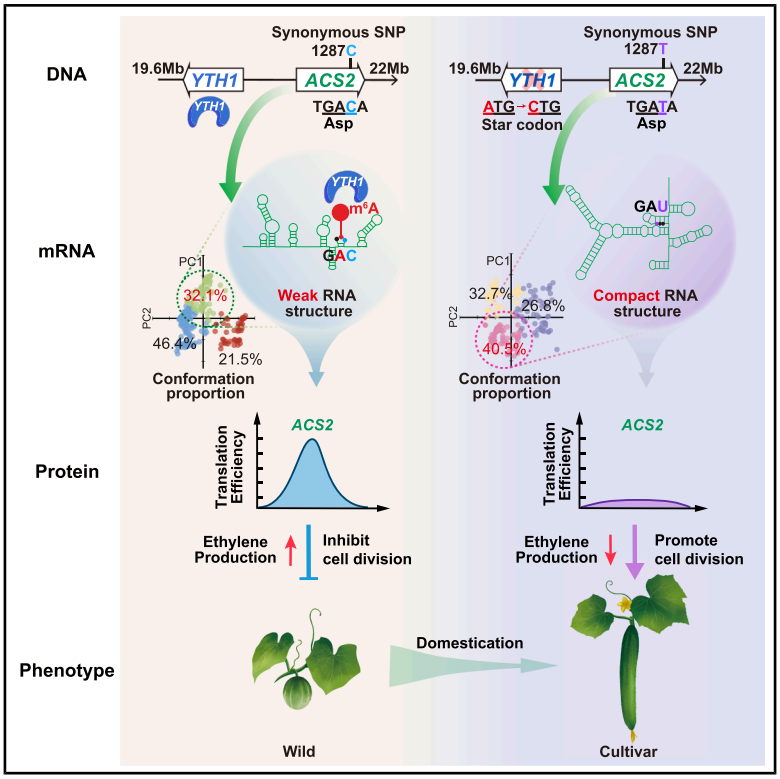

Highlights

- Two epistatically interacting genes, *YTH1* and *ACS2*, confer cucumber domestication
- The 1287C>T synonymous mutation of *ACS2* is the causative variant
- 1287T disrupts nearby m^{6}A methylation and forms a compact RNA structure of *ACS2*
- m^{6}A results in weaker conformation of RNA structure and enhances translation efficiency

Authors

Tongxu Xin, Zhen Zhang, Yueying Zhang, ..., Yiliang Ding, Sanwen Huang, Xueyong Yang

Correspondence

yiliang.ding@jic.ac.uk (Y.D.), huangsanwen@caas.cn (S.H.), yangxueyong@caas.cn (X.Y.)

In brief

A synonymous mutation in aminocyclopropane-1-carboxylic acid synthase controls cucumber fruit length domestication by disrupting m^{6}A modification and forming a compact RNA structure, highlighting how synonymous mutations shape the biological traits through epitranscriptomic regulations.

Xin et al., 2025, Cell *188*, 1–13
August 21, 2025
https://doi.org/10.1016/j.cell.2025.06.007

CellPress

Cell

CellPress
OPEN ACCESS

Article

Recessive epistasis of a synonymous mutation confers cucumber domestication through epitranscriptomic regulation

Tongxu Xin,[1,9] Zhen Zhang,[2,3,9] Yueying Zhang,[4,9] Xutong Li,[1,9] Shenhao Wang,[1] Guanqun Wang,[5] Haoxuan Li,[5] Bowen Wang,[1,2] Mengzhuo Zhang,[1] Wenjing Li,[1] Haojie Tian,[1] Zhonghua Zhang,[6] Yu-Lan Xiao,[7,8] Weixin Tang,[7,8] Chuan He,[5] Yiliang Ding,[4,*] Sanwen Huang,[2,*] and Xueyong Yang[1,10,*]

[1]State Key Laboratory of Vegetable Biobreeding, Institute of Vegetables and Flowers, Chinese Academy of Agricultural Sciences, Beijing 100081, China
[2]Shenzhen Branch, Guangdong Laboratory of Lingnan Modern Agriculture, Genome Analysis Laboratory of the Ministry of Agriculture and Rural Affairs, Agricultural Genomics Institute at Shenzhen, Chinese Academy of Agricultural Sciences, Shenzhen 518120, China
[3]State Key Laboratory of Crop Stress Adaptation and Improvement, College of Agriculture, Henan University, Jinming Avenue 1, Kaifeng 475004, China
[4]Department of Cell and Developmental Biology, John Innes Centre, Norwich Research Park, Norwich NR4 7UH, UK
[5]Department of Chemistry, Department of Biochemistry and Molecular Biology, Institute for Biophysical Dynamics, Howard Hughes Medical Institute, University of Chicago, Chicago, IL 60637, USA
[6]Engineering Laboratory of Genetic Improvement of Horticultural Crops of Shandong Province, College of Horticulture, Qingdao Agricultural University, Qingdao 266109, China
[7]Department of Chemistry, The University of Chicago, Chicago, IL, USA
[8]Institute for Biophysical Dynamics, The University of Chicago, Chicago, IL, USA
[9]These authors contributed equally
[10]Lead contact
*Correspondence: yiliang.ding@jic.ac.uk (Y.D.), huangsanwen@caas.cn (S.H.), yangxueyong@caas.cn (X.Y.)
https://doi.org/10.1016/j.cell.2025.06.007

SUMMARY

Synonymous mutations, once known as "silent" mutations, are increasingly attracting the interest of biologists. Although they may affect transcriptional or post-transcriptional processes, their impact on biological traits remains under-investigated, particularly at the organismal level. Here, we identified two closely linked, epistatically interacting genes: *YTH1*, an RNA N^6-methyladenosine (m^6A) reader, and *ACS2*, an *aminocyclopropane-1-carboxylic acid* (ACC) synthase, which contribute to cucumber fruit length domestication. The causative mutation in *ACS2* is a synonymous substitution at 1287C>T. In wild cucumber, $ACS2^{1287C}$ results in m^6A modification on nearby adenosine residues and the formation of loose RNA structural conformations. YTH1 recognizes the m^6A modification, alters the folding equilibrium toward the weakest RNA structural conformation, and increases the *ACS2* protein level, resulting in shorter fruit. In cultivated cucumber, $ACS2^{1287T}$ disrupts m^6A methylation and forms compact RNA structural conformations, leading to attenuated protein production and fruit elongation. This study provides genetic evidence of synonymous variation shaping a biological trait through epitranscriptomic regulations.

INTRODUCTION

A synonymous mutation is a change in the coding DNA sequence that does not alter the encoded amino acid. Compared with non-synonymous mutations, which change protein sequences, it has long been thought that most synonymous mutations are biologically silent,[1] with a few exceptions. Some human disorders have been linked to synonymous mutations.[2,3] A recent study in yeast showed that most synonymous mutations resulted in a significant reduction in fitness, as did non-synonymous mutations,[4] although somewhat controversial.[5] Notably, recent large-scale phylogenomic analyses in members of Solanaceae have revealed a large number of synonymous mutations are evolutionarily constrained.[6] Studies showed that some synonymous positions may influence several transcriptional and post-transcriptional processes, including mRNA splicing, tRNA selection, and translation efficiency (TE).[7–9] Furthermore, *in vitro* studies found that non-coding variants, such as synonymous mutations associated with diverse human diseases and phenotypes, can alter RNA structures and impact RNA functions.[10,11] Although these findings suggest that synonymous changes play a role in cellular function and organismal

fitness, there is nonetheless little genetic evidence in multicellular organisms of synonymous mutations shaping biological traits or the associated modes of action.

N^6-methyladenosine RNA (m^6A) is a prevalent messenger RNA modification in eukaryotes.[12] The modification is preferentially present in a subset of the RRACH consensus sites (R, purine; H, non-guanine base) and is enriched around stop codons, in the 3′ untranslated regions (3′ UTRs), or within long internal exons through the action of a "writer": an m^6A methyltransferase complex.[13,14] m^6A has been demonstrated to regulate multiple post-transcriptional processes, including mRNA stability and translation,[15,16] in part through the action of m^6A reader proteins, including members of the conserved YTH protein family.[17] The m^6A erasers, fat mass and obesity-associated factor (FTO),[18,19] and the alkylated DNA repair protein AlkB homologs (ALKBH5 in mammals and ALKBH9B or ALKBH10B in plants)[20,21] can convert m^6A into adenosine. Recent studies suggest that m^6A modification may influence biological processes through its strong association with RNA structure.[22,23] However, it remains unclear how m^6A affects RNA structure, largely due to challenges in dissecting the heterogeneity of RNA conformations. While m^6A is known to regulate post-transcriptional gene expression, direct genetic evidence linking m^6A to specific biological outcomes remains limited.

Here, we discovered two closely linked, epistatically interacting loci associated with cucumber fruit length domestication. Subsequent genetic and molecular analyses generated an organismal example of synonymous mutation controlling domesticated traits through m^6A modification and RNA structure-mediated epitranscriptomic regulations.

RESULTS

Two closely linked, interacting genes related to fruit length domestication

Fruit length, which is strongly correlated with yield, is a domestication trait (Figure S1A). We previously detected a fruit length quantitative trait locus (QTL), *FL1*, within the domestication sweep region on chromosome 1.[24] To map the causal gene(s) at the *FL1* locus, backcross introgression lines (ILs) were developed in which chromosome segments of wild cucumber (*C. sativus* var. *hardwickii* PI183967), which bears short and round fruit, were introduced into cultivated cucumber (*C. sativus* cv. Xintaimici) that has typical elongated fruit (Figures 1A, S1B, and S1C). IL-1-1, carrying a fragment of *hardwickii* chromosome 1 covering the *FL1* locus, had fruits that were 40% shorter than those from Xintaimici (Figures 1A, S1C, and S1D). All the F_1 progeny derived from a cross between Xintaimici and IL-1-1 had an intermediate-length fruit phenotype compared with their parents (Figures S1E and S1F), and the F_2 segregation pattern fitted a Mendelian ratio of 1:2:1 (Figure S1F), indicating that *FL1* could be a single semi-dominant locus.

We next created an 8,000-individual F_2 population by crossing IL-1-1 with Xintaimici for fine mapping (Figure S1E). Two closely linked and epistatically interacting loci, *FL1.1* and *FL1.2*, were detected. Genetic analysis also showed that $FL1.1^W$ and $FL1.2^W$ were dominant over $FL1.1^C$ and $FL1.2^C$ (Figure S1G). *FL1.1* and *FL1.2* were narrowed to a 586 kb region and a 278 kb region using a map-based cloning strategy (Figures 1B and 1C). Compared with $FL1.1^W$ $FL1.2^W$ plants, which had the shortest fruits, the mean fruit length of $FL1.1^W$ $FL1.2^C$ and $FL1.1^C$ $FL1.2^W$ plants increased by about 70% and 30%, respectively (Figures 1D and 1E), indicating that both $FL1.1^C$ and $FL1.2^C$ contribute to fruit elongation. Interestingly, the $FL1.1^C$ $FL1.2^C$ fruits were 72% longer than those of $FL1.1^W$ $FL1.2^W$, and the loci did not show an additive effect, but like the case with $FL1.1^W$ $FL1.2^C$ (Figures 1D and 1E). Thus, when the $FL1.2^C$ allele was present, regardless of the type of *FL1.1* allele, fruit length was determined by $FL1.2^C$, indicating that $FL1.2^C$ is recessively epistatic to *FL1.1* (Figure 1F). We further found that the fruit length phenotype could be attributed to a decreased cell number (Figure 1G), while the average cell size showed no significant difference among the four genotypes (Figures S1H and S1I). Thus, the reduced fruit elongation phenotype underlying the *FL1* locus in wild cucumber is caused by two closely linked, epistatically interacting genes.

FL1.2 is defined by a synonymous mutation in the *ACS2* gene

Since $FL1.2^C$ is epistatic to *FL1.1*, and $FL1.1^W$ $FL1.2^C$, and $FL1.1^W$ $FL1.2^W$ showed the greatest difference in fruit length (Figure 1E), we first used these two genotype materials, with the unchanged $FL1.1^W$, to clone *FL1.2*. Recombinant events in the *FL1.2* region were generated by backcrossing IL-1-1-1 to Xintaimici, and the region of interest was narrowed to a 17.3 kb interval, which had only one annotated gene, *Csa1G580750* (Figure 2A). This corresponds to an *aminocyclopropane-1-carboxylic acid synthase* (*ACS2*) gene that we previously found controls ethylene dose-dependent fruit elongation.[25] Genomic sequencing of *ACS2* in $FL1.1^W$ $FL1.2^W$ and $FL1.1^W$ $FL1.2^C$ plants revealed a three-base insertion in the 5′ UTR of $ACS2^W$, two SNPs in the introns, and three synonymous SNPs in the exons (Figure 2A). Full-length transcriptome sequencing and RNA sequencing (RNA-seq) using female flowers from near-isogenic lines (NILs) showed that these variants did not affect RNA splicing and gene expression (Figure S2A). Quantitative reverse transcription-polymerase chain reaction (RT-qPCR) analysis also revealed that the expression of *ACS2* showed no significant difference between $FL1.1^W$ $FL1.2^W$ and $FL1.1^W$ $FL1.2^C$ plants during ovary development (Figure S2B). However, immunoblotting assay using anti-ACS2 antibody[25] found that the ACS2 protein level was significantly higher in $FL1.1^W$ $FL1.2^W$ compared with $FL1.1^W$ $FL1.2^C$ plants (Figure 2B).

To determine which of the genetic variations could affect protein levels, a translational activity assay was performed, using a dual-luciferase system to examine the potential regulatory activities and significance of the 5′ UTR insertion and the three synonymous SNPs. The eight combinations of 5′ UTR and/or $ACS2^W$ coding sequence (CDS) and/or $ACS2^C$ CDS were separately cloned upstream from the firefly luciferase (FLuc) coding region in an expression cassette, driven by the 35S promoter. A 35S-promoter-driven cassette expressing the Renilla luciferase (RLuc) was used as an internal vector control. The constructs were transiently expressed in cucumber cotyledons. We observed a significant increase of FLuc/RLuc activities in these constructs harboring the $ACS2^W$ CDS, while those containing

Please cite this article in press as: Xin et al., Recessive epistasis of a synonymous mutation confers cucumber domestication through epi-transcriptomic regulation, Cell (2025), https://doi.org/10.1016/j.cell.2025.06.007

CellPress
OPEN ACCESS

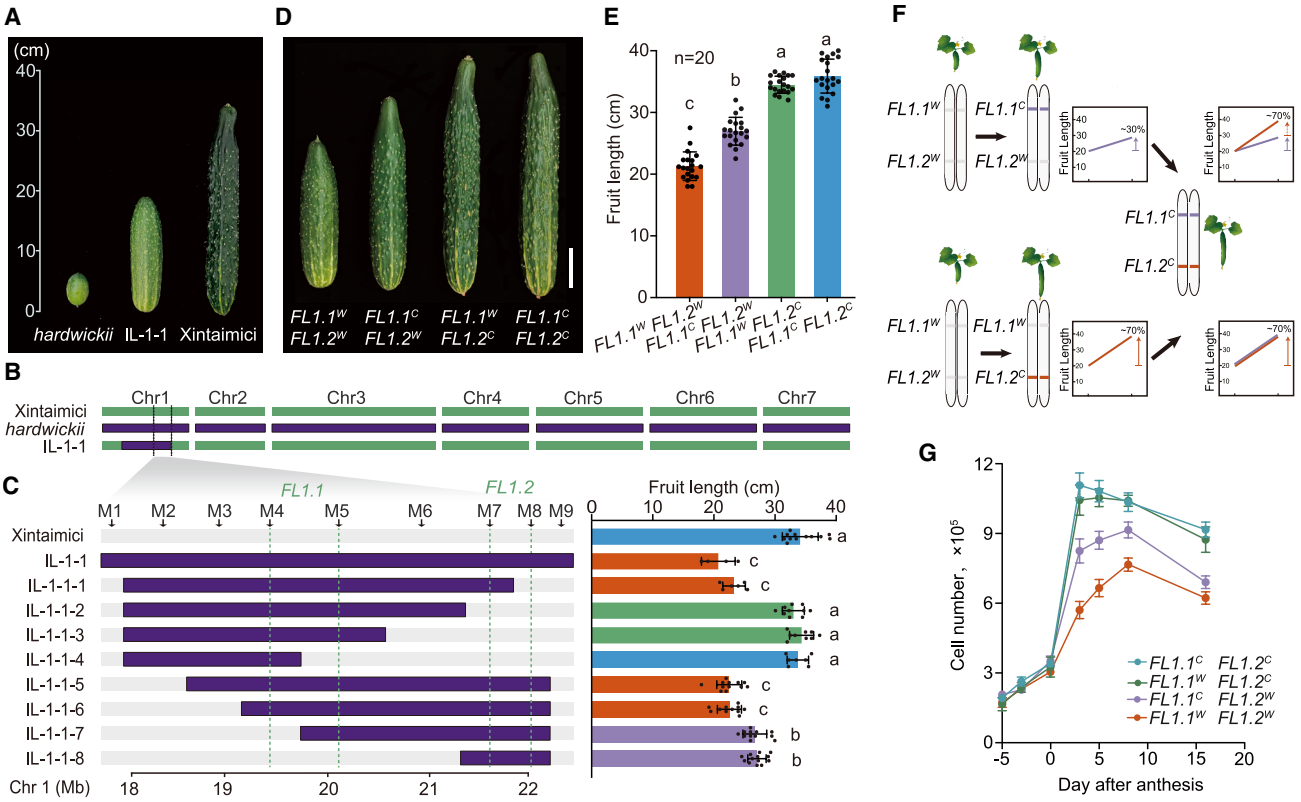

Figure 1. Two closely linked, interacting genes related to fruit length domestication

(A) Representative fruits of the wild cucumber *hardwickii* (left), the cultivated cucumber Xintaimici (right), and an IL-1-1 (middle).

(B) Representative introgression and parental line genotypes. Green and purple, Xintaimici and *hardwickii* genotypes, respectively.

(C) Identification and mapping of the two interacting loci *FL1.1* and *FL1.2* by breaking the IL-1-1 introgression fragment into smaller fragments (IL-1-1-1 to IL-1-1-8). Left, genotypes of selected recombinants. Gray and purple, Xintaimici and *hardwickii* genotypes, respectively. Vertical green dotted lines define the genetic interval of *FL1.1* and *FL1.2*. M1–M9 represent the SNP markers (Table S1). Right, fruit length of corresponding recombinant plants. Data are mean ± SD (*n*, number of fruits from different plants). Different letters indicate significant differences ($p < 0.05$, one-way ANOVA and Tukey's test).

(D) Representative fruit phenotypes of the four genotypes. W and C superscripts stand for wild and cultivar alleles, respectively. Scale bar, 5 cm.

(E) Quantification of fruit length related to (D). Data are mean ± SD ($n = 20$). Different letters indicate significant differences ($p < 0.05$, one-way ANOVA and Tukey's test).

(F) Schematic diagram showing that $FL1.2^C$ is genetically recessive, epistatic to *FL1.1*. Purple and red represent the $FL1.1^C$ and $FL1.2^C$ genotypes, respectively.

(G) The cell number analysis on the four genotypes. Data are means ± SD ($n = 3$).

See also Figure S1.

$ACS2^W$ 5′ UTR showed no effects, and since the relative mRNA expression levels of *ACS2* were approximately equivalent for all constructs, we concluded that one of the synonymous variants likely determined the augmented protein level of the $ACS2^W$ allelic gene (Figure 2C). To determine which of the three synonymous mutations could be causative, eight combinations of the three SNPs were created for and used in the dual-luciferase assays. Only constructs with the third synonymous SNP C^{1287} from the $ACS2^W$ gene exhibited higher FLuc/RLuc activities, with all constructs showing no difference in mRNA expression levels, suggesting a major effect of the third synonymous SNP C^{1287} in promoting TE (Figure 2D). We also excluded the effect of SNP variants in introns, determining that they have no effect on ACS2 protein levels (Figure S2C). These results suggested that the 1287C>T synonymous mutation controlled the observed ACS2 protein levels.

We then analyzed the distribution of *ACS2* T^{1287} and C^{1287} SNPs in 115 cucumber core accessions, with the C^{1287} variant only present in wild cucumbers (India group), indicating human selection of T^{1287} in cultivated cucumber during domestication (Figure S2D). To demonstrate that the 1287C>T synonymous SNP was in fact the causal genetic mutation for *FL1.2*, 1287C and 1287T constructs, containing a 2-kb region of the native promoter plus the full-length CDS of *ACS2* with only one synonymous variant at the 1287 position, were transformed into the $FL1.1^W$ $FL1.2^C$ and $FL1.1^C$ $FL1.2^C$ plants, respectively (Figure S2E). To exclude the possibility that dose effects resulted from differences in the gene copy number of the *ACS2* gene,[25] transgenic plants with single copies were selected using Southern blot analysis to observe the phenotype (Figure S2F). In both backgrounds, transgenic plants carrying the wild $ACS2^{1287C}$ allele bore significantly shortened fruit compared with those

Please cite this article in press as: Xin et al., Recessive epistasis of a synonymous mutation confers cucumber domestication through epi-transcriptomic regulation, Cell (2025), https://doi.org/10.1016/j.cell.2025.06.007

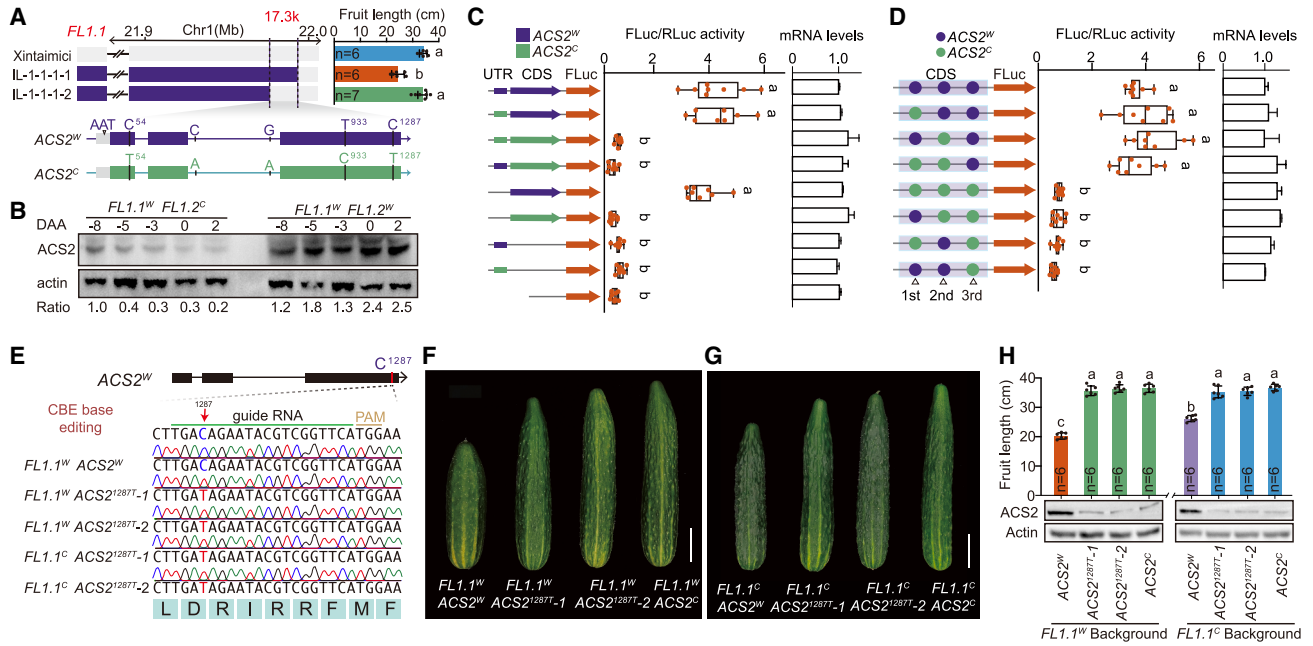

Figure 2. *FL1.2* is defined by a synonymous mutation in the *ACS2* gene

(A) The *FL1.2* fine-mapping interval includes the *ACS2* gene (*Csa1G580750*). Upper: genotypes and fruit length of selected recombinants. Data are mean ± SD (*n*, number of fruits from different plants). Different letters indicate significant differences ($p < 0.05$, one-way ANOVA and Tukey's test). Gray and purple, Xintaimici and *hardwickii* genotypes, respectively. Lower: a schematic diagram showing the $ACS2^W$ and $ACS2^C$ gene structure and variants. The boxes, lines, and gray boxes represent exons, introns, and UTRs, respectively.

(B) Immunoblotting assay showing the *ACS2* protein levels during early fruit development.

(C) Functional identification of the 5′ UTR or CDS variations of *ACS2* using dual-luciferase reporter assays. Left, schematic showing the constructs with all combinations of 5′ UTR and CDS variations in $ACS2^W$ and $ACS2^C$. Middle: FLuc/RLuc activities of the corresponding constructs are shown on the left. Data are means ± SD ($n = 8$). Different letters indicate significant differences ($p < 0.05$, one-way ANOVA and Tukey's test). Right, relative *ACS2* mRNA expression levels from the corresponding constructs. Data are means ± SD ($n = 3$).

(D) Functional identification of the three synonymous SNPs using dual-luciferase reporter assays. Left, schematic showing the constructs with different combinations of the three synonymous SNPs in $ACS2^W$ and $ACS2^C$. The three dots represent the three synonymous SNPs. Middle: FLuc/RLuc activity of the corresponding constructs is shown on the left. Data are means ± SD ($n = 8$). Different letters indicate significant differences ($p < 0.05$, one-way ANOVA and Tukey's test). Right, relative *ACS2* mRNA expression levels from the various constructs. Data are means ± SD ($n = 3$).

(E) The base editing results of $ACS2^{1287C}$.

(F and G) The fruit length of transgenic plants with C^{1287} to T transitions. Scale bar, 5 cm.

(H) Quantification of fruit length and ACS2 protein levels related to (F) and (G). Data are mean ± SD ($n = 6$). Different letters indicate significant differences ($p < 0.05$, one-way ANOVA and Tukey's test).

See also Figure S2.

with the cultivated allele $ACS2^{1287T}$, demonstrating the role of the C^{1287} mutation in controlling fruit length (Figures S2G–S2I). Additionally, we observed that transgenic $ACS2^{1287C}$ plants produced much shorter fruit when $FL1.1^W$ $FL1.2^C$ was used as a recipient than when $FL1.1^C$ $FL1.2^C$ was used, further highlighting the observation that $FL1.1^W$ interacts with $ACS2^W$ (Figures S2G–S2I).

We also examined the genome sequence around this SNP and found that the cytosine base editing (CBE) tool could be applied to target the synonymous C^{1287} for a C to T transition. We then established an effective CBE base editing system in cucumber to genetically verify the functionality of the C^{1287} mutation directly. Homozygous-edited T_1 generation plants in the $FL1.1^W$ $FL1.2^W$ and $FL1.1^C$ $FL1.2^W$ backgrounds were obtained (Figure 2E). In both backgrounds, the C to T transition significantly reduced ACS2 protein abundance and promoted fruit elongation, demonstrating that the 1287C>T synonymous mutation is the causative SNP for *FL1.2* and fruit length increase during domestication (Figures 2F–2H).

FL1.1 is defined by a deleterious mutation in the *YTH1* gene

To fine-clone *FL1.1*, we produced recombinants in the *FL1.1* region by backcrossing IL-1-1-6 to Xintaimici. We localized *FL1.1* to an 11 kb interval that had one annotated candidate, *Csa1G538270*, which encodes the RNA m^6A reader protein, YTH1 (Figures 3A and S3A). Genomic sequencing analysis revealed that, unlike *hardwickii*, Xintaimici has an A to C SNP in the initiation codon that changes the start position of the predicted open reading frame, thereby abolishing the YTH domain (Figures 3B–3D). Full-length transcriptome and RT-qPCR analyses showed that the mutation did not affect the mRNA splicing

Please cite this article in press as: Xin et al., Recessive epistasis of a synonymous mutation confers cucumber domestication through epi-transcriptomic regulation, Cell (2025), https://doi.org/10.1016/j.cell.2025.06.007

CellPress
OPEN ACCESS

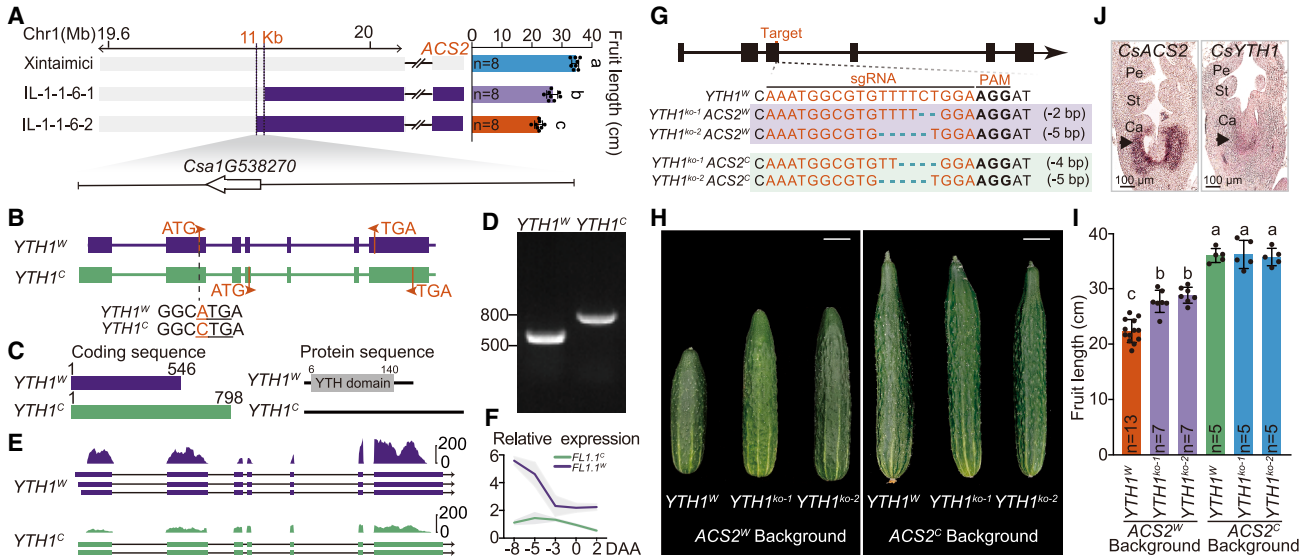

Figure 3. *FL1.1* is defined by a deleterious mutation in the *YTH1* gene

(A) The *FL1.1* fine-mapping interval includes the *YTH1* gene (*Csa1G538270*). Upper: genotypes and fruit length of selected recombinants. Gray and purple, Xintaimici and *hardwickii* genotypes, respectively. Data are means ± SD (n = 8). Different letters indicate significant differences ($p < 0.05$, one-way ANOVA and Tukey's test).

(B) The *YTH1* gene structure and variants. The sequence below is the base around the initiation codon.

(C) The length of CDS and protein sequences in $YTH1^W$ and $YTH1^C$. The numbers represent the beginning and end of the CDS and YTH protein domains.

(D) PCR showing the length of CDS in $YTH1^W$ and $YTH1^C$.

(E and F) Full-length transcriptome (E) and RT-qPCR (F) showed the splicing and expression of mRNA. (F) Colored lines indicate median expression, with the gray area representing the 5th and 95th quantiles.

(G) Generation of $YTH1^{ko}$ null mutants by CRISPR-Cas9 using a single-guide RNA. sgRNA target and PAM are indicated in red and bold font, respectively. The deletions are indicated in blue dashes.

(H and I) The fruit length of $YTH1^{ko}$ mutants. Scale bar, 5 cm. Data are means ± SD. n, number of fruits from different plants. Different letters indicate significant differences ($p < 0.05$, one-way ANOVA and Tukey's test).

(J) *In situ* hybridization experiment showing the expression of *ACS2* and *YTH1* mRNA in carpels of developing ovaries. Pe, petal; St, stamen; Ca, carpel. Scale bar, 100 μm.

See also Figure S3.

but did result in significantly lower YTH1 transcript levels in Xintaimici (Figures 3E and 3F). We expressed $YTH1^W$-green fluorescent protein (GFP) as a recombinant protein in *Nicotiana benthamiana* leaf cells and observed by confocal microscopy that it accumulated in both the nucleus and the cytosol (Figure S3B).

Since $YTH1^W$ is the dominant allelic gene, to validate the function of *YTH1*, we used the CRISPR-Cas9 gene editing system to knock out $YTH1^W$ in the $FL1.1^W$ $FL1.2^W$ and $FL1.1^W$ $FL1.2^C$ backgrounds (Figure 3G). The fruit length of the resulting $YTH1^{ko}$ plants increased by 25% in the $FL1.1^W$ $FL1.2^W$ background, but no effect was observed in the $FL1.1^W$ $FL1.2^C$ background. These results demonstrated that *YTH1* is the underlying $FL1.1^W$ gene and also indicated the recessive epistatic effect of $ACS2^C$ ($FL1.2^C$) on *YTH1* (Figures 3H and 3I).

We next investigated the distribution of *YTH1* and *ACS2* alleles in 115 cucumber core accessions. The results revealed that the $ACS2^C$ allele was subjected to strong selection in cultivated cucumber (Eurasian and East Asian types) during domestication (Figures S3C and S3D). Meanwhile, $YTH1^W$ and $YTH1^C$ alleles were evenly distributed among the populations, showing the comparable fixation of $YTH1^W$ $ACS2^C$ and $YTH1^C$ $ACS2^C$ in both Eurasian and East Asian types (Figure S3D). We did not find $YTH1^C$ $ACS2^W$ genotype in cucumber populations, indicating a one-step selection on $ACS2^C$, which coincided with the result from the selective sweep (Figure S3E). We also examined the expression patterns of *YTH1* and *ACS2* using *in situ* hybridization. Both genes were expressed in developing carpels, with $ACS2^W$ preferentially expressed in the carpel margin and $YTH1^W$ expressed in the whole carpel (Figure 3J), thus showing an overlap in spatiotemporal expression.

The 1287C>T synonymous mutation modulates *ACS2* mRNA m^{6}A methylation and the protein TE

Since YTH has been shown to preferentially bind to mRNA and affect mRNA stability by regulating degradation or TE by promoting ribosome loading,[15,16] to investigate the mechanism of epistatic interaction involving *YTH1* and *ACS2* in fruit elongation, we detected potential interactions between *YTH1* and *ACS2* mRNA. $YTH1^W$-*Myc* and $YTH1^C$-*Myc* were overexpressed in the $YTH1^C$ $ACS2^W$ and $YTH1^C$ $ACS2^C$ backgrounds, respectively (Figures S4A and S4B), followed by formaldehyde cross-linking and immunoprecipitation (FA-CLIP)[26] to map the transcripts bound by YTH1 using the female flower buds. $YTH1^W$ binding sites were observed to be highly reproducible in the

two biological replicates (Figure S4C). Peaks close to the third synonymous mutation of *ACS2* mRNA were exclusively enriched in *YTH1*^{W}*-Myc ACS2*^{W}, suggesting that the functional YTH1^{W} bound to *ACS2*^{W} mRNA but not *ACS2*^{C} mRNA (Figure 4A).

Given that YTH can recognize m^{6}A-modified mRNAs, we hypothesized that the 1287C>T synonymous mutation affects the m^{6}A modification level of the *ACS2* transcript around the mutation and alters *ACS2* TE. To test this, we first performed antibody-based m^{6}A profiling and RNA-seq (m^{6}A-seq) using *YTH1*^{W} *ACS2*^{W} and *YTH1*^{W} *ACS2*^{C} ovaries. m^{6}A peaks from two independent biological replicates were highly reproducible and were abundant near the stop codon and 3′ UTR (Figures S4D and S4E). We analyzed the top 1,000 most significant peaks and found at least one m^{6}A consensus sequence RRACH in over 90% of peaks (Figure S4F). The *YTH1*^{W} *ACS2*^{W} mRNA exhibited an enriched m^{6}A peak on the third exon of *ACS2* (Figure 4B).

To further survey the *in planta* effects of *YTH1* and the *ACS2* 1287C>T synonymous mutation on m^{6}A modification, we developed four isogenic lines, *YTH1*^{W} *ACS2*^{1287C} (*WW*), *YTH1*^{ko} *ACS2*^{1287C} (*KW*), *YTH1*^{W} *ACS2*^{1287T} (*WC*), and *YTH1*^{ko} *ACS2*^{1287T} (*KC*), among which the only difference was in the *YTH1* gene and the *ACS2* 1287C>T synonymous mutation (Figure 4C). We then performed m^{6}A-RNA immunoprecipitation (RIP)-qPCR, using *CsNADH* as the internal control.[26] Both *WW* and *KW* ovaries showed substantial m^{6}A levels on *ACS2* compared with *WC* and *KC*, while *YTH1* expression did not show significant effects on the m^{6}A level (Figure 4D). To test whether the transient overexpression of the *ACS2*^{1287C} gene could also promote its accumulation of m^{6}A methylation, we expressed *35S::ACS2*^{1287C} and *35S::ACS2*^{1287T}, the constructs carrying only the 1287C>T synonymous change, in cucumber cotyledons, respectively. We confirmed that the overexpressed *ACS2*^{1287C} mRNA exhibited a greater degree of m^{6}A methylation compared with *ACS2*^{1287T} (Figure 4E).

We then performed ACS2 immunoblotting assays for the four genotypes during early fruit development and observed that the *WW* plants exhibited higher ACS2 protein levels (Figures 4F and S4G–S4I). Notably, disruption of the *YTH1* gene suppressed the protein production of *ACS2*^{1287C} in *KW* plants, while ACS2 protein levels were further impaired in both *WC* and *KC* plants (Figure 4F). The translational efficiency of *ACS2* mRNA in *WW*, *KW*, *WC*, and *KC* plants was further examined by ribosome profiling (Figures S4J and S4K), showing that *ACS2*^{1287C} mRNA TE in *WW* and *KW* plants was higher than in plants with the *ACS2*^{1287T} allele (both *WC* and *KC*) (Figure 4G). Also, the disruption of *YTH1* in *KW* caused a significant decrease in *ACS2* TE compared with that in *WW*, while there was no difference in TE between *WC* and *KC* (Figure 4G), revealing the regulatory mechanism underlying the recessive epistasis of *ACS2*^{1287T} to *YTH1*. We next established that fruit ethylene production was positively correlated with ACS2 protein levels in the four genotypes but negatively correlated with fruit length (Figure S4L), consistent with our previous results revealing ethylene dose-dependent fruit elongation.[25] These results indicated that the synonymous *ACS2*^{1287C} SNP in wild cucumber promotes its m^{6}A methylation and TE, and the interaction with YTH1 further leads to a boost of TE of *ACS2*^{1287C}.

We then employed evolved TadA-assisted N^6-methyladenosine sequencing (eTAM-seq) to detect the *ACS2* mRNA m^{6}A modification at single-based resolution.[27] We checked the global conversion efficiency across the samples and found the results of single-base resolution detection are reliable and repeatable (Figure S4M). The m^{6}A sites are also enriched around stop codons, consistent with m^{6}A-seq methods, and a clear DRACH motif emerges in sequences surrounding m^{6}A (Figures S4N and S4O). The site-specific amplification around the third exon of *ACS2* was then performed to detect and quantify its m^{6}A modifications at single-base resolution. In the stable transgenic materials, the *WW* plant showed greater m^{6}A methylation at the A^{1286} (around 10%) close to the 1287C>T SNP and also several surrounding adenines in the 5′ direction from the synonymous SNP with a low ratio (around 3%) compared with the *WC* plant (Figure 4H). Due to the very low expression level of *ACS2* gene, which specifically expresses in the carpel of female flowers at early stage, the result was further confirmed by other methods. Firstly, the single-base elongation- and ligation-based qPCR amplification method (SELECT) was used to verify the m^{6}A signal on A^{1286} *in vivo*, along with several adenines in the 5′ direction as controls, at the single-base level.[28] We first cloned the cucumber m^{6}A demethylase gene *CsALKBH10B*, based on the sequence homology with *AtALKBH10B*[20] in *Arabidopsis thaliana*, and confirmed its m^{6}A demethylation function in cucumber (Figures S4P and S4Q). The SELECT results showed that the presence of ALKBH10B significantly promoted the production of the final elongated and ligated products when using mRNA of *WW* plant as the template, further confirming the existence of m^{6}A on A^{1286} in *ACS2*^{1287C}, but not in *ACS2*^{1287T} (Figure 4I). We also showed that except for a faint signal on A^{1262}, no m^{6}A methylation was observed on the other selected adenines (Figure S4R). Meanwhile, we also used absolute quantification to determine the m^{6}A methylation level at A^{1286} base on the known concentrations of RNA spike-in[29] (Figure S4S), and the result showed that there was nearly 18% m^{6}A modification level at A^{1286} site, which could be significantly erased by demethylase ALKBH10B (Figure 4J). These results all point to the presence of m^{6}A modification on A^{1286} of *ACS2*^{1287C} transcripts, which is determined by the adjacent synonymous mutation C^{1287}.

The 1287C>T synonymous mutation changes the TE of *ACS2* via m^{6}A modification and RNA structural alterations

To determine the *in planta* effect of YTH1 binding and m^{6}A modification on target gene TE, we categorized the *WW* transcripts according to m^{6}A-seq and FA-CLIP into three groups[30]: m^{6}A-modified targets, m^{6}A-modified transcripts bound by YTH1, and non-targets (absent from both m^{6}A-seq and FA-CLIP) (Figure S5A). We found a notable increase in TE for m^{6}A-modified transcripts in *WW* compared with in *KW*, particularly for the YTH1-bound and m^{6}A-modified transcripts (Figure S5B).

Since the transient expression system in cotyledon was demonstrated to be effective in modulating levels of m^{6}A modification of target transcripts and protein level quantification (Figures 2C, 2D, and 4E), we then explore the molecular mechanism of the synonymous mutation in enhancement of *ACS2*^{1287C}

Please cite this article in press as: Xin et al., Recessive epistasis of a synonymous mutation confers cucumber domestication through epi-transcriptomic regulation, Cell (2025), https://doi.org/10.1016/j.cell.2025.06.007

CellPress
OPEN ACCESS

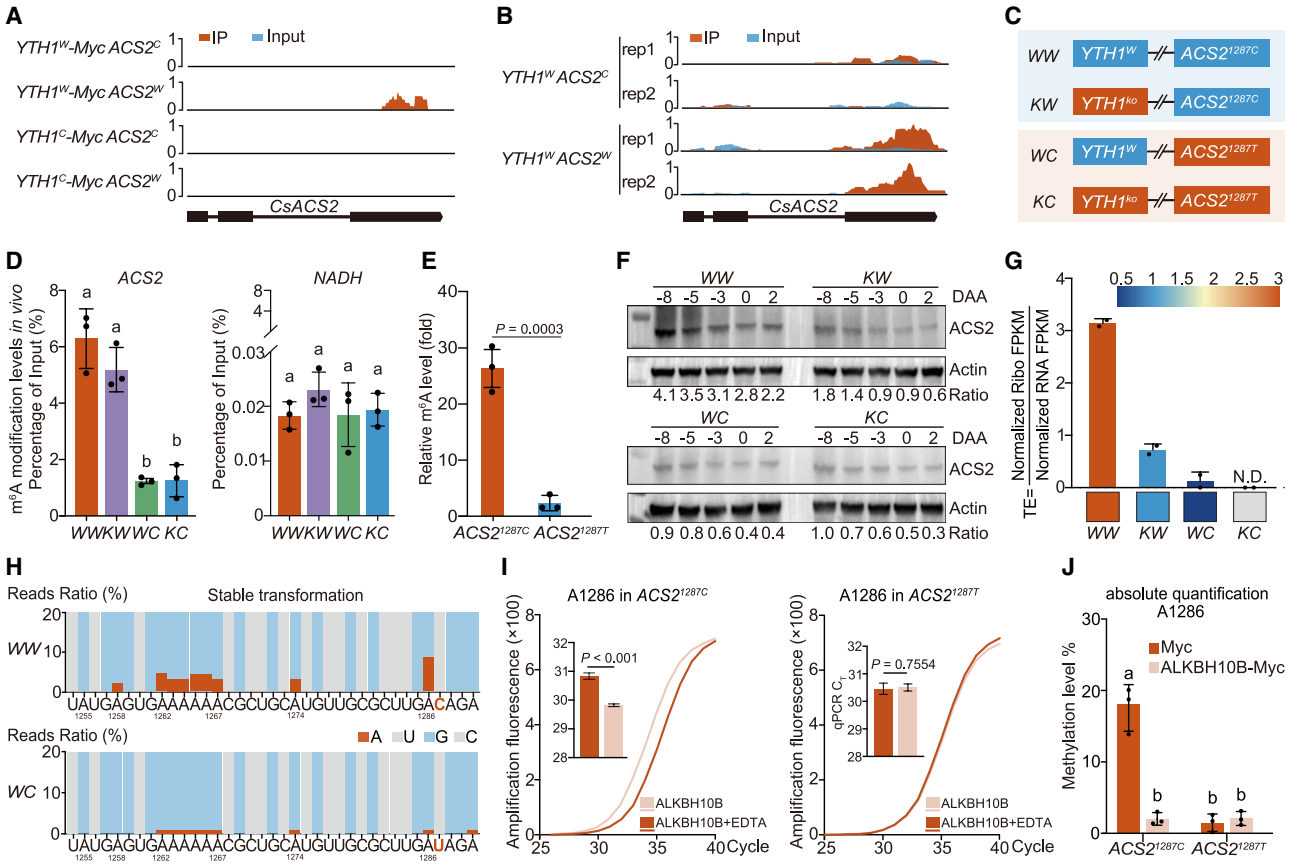

Figure 4. The 1287C>T synonymous mutation modulates *ACS2* mRNA m^{6}A methylation and the protein TE

(A) FA-CLIP enrichment peak coverage of *ACS2* mRNA.

(B) m^{6}A-seq enrichment peak coverage of *ACS2* mRNA.

(C) Development of four isogenic lines with only differences in the *YTH1* gene and *ACS2* 1287 synonymous mutations.

(D) Relative m^{6}A levels of *ACS2* (left) and *NADH* (right, as a control) in isogenic lines *WW*, *KW*, *WC*, and *KC* detected by m^{6}A-RIP-qPCR. Data are means ± SD (n = 3). Different letters indicate significant differences ($p < 0.05$, one-way ANOVA and Tukey's test).

(E) Relative m^{6}A levels in *35S::ACS2^{1287C}* and *35S::ACS2^{1287T}* detected by m^{6}A-RIP-qPCR. Data are means ± SD (n = 3). p value was calculated using a two-sided t test.

(F) Immunoblotting assays of ACS2 protein levels in four isogenic lines.

(G) Relative TE of ACS2 in *WW*, *KW*, *WC*, and *KC* by ribosome profiling. n = 2 biological replicates. Lower: the corresponding heat map of TE.

(H) Detection of m^{6}A modification around 1287 synonymous SNPs of *ACS2* mRNA at single-base resolution level. The letter in red and bold represents the 1287 synonymous mutations.

(I) The SELECT results for detecting m^{6}A modification at the A^{1286} in *ACS2^{1287C}* (left) and *ACS2^{1287T}* (right). Data are mean ± SD (n = 3). p value was calculated using a two-sided t test.

(J) Absolute quantification RT-PCR result showing the m^{6}A modification level at A^{1286} in *ACS2^{1287C}*. Data are means ± SD (n = 3). Different letters indicate significant differences ($p < 0.05$, one-way ANOVA and Tukey's test).

See also Figure S4.

TE using *35S::ACS2^{1287C}* and *35S::ACS2^{1287T}* fused with the luciferase reporter gene and transiently co-expressed in cucumber with *35S::YTH1^W-Myc*, *35S::ALKBH10B*, or with a control vector, respectively (Figure S5C).

Significant enrichment of m^{6}A modification was detected on *ACS2^{1287C}* compared with *ACS2^{1287T}* using an m^{6}A-RIP-qPCR assay (Figure 5A), and the increased protein level of *ACS2^{1287C}* was observed (Figure 5C). The co-expression of *YTH1^W-Myc* did not affect the m^{6}A level on *ACS2^{1287C}* (Figure 5A); however, YTH1^W preferentially bound to *ACS2^{1287C}* compared with *ACS2^{1287T}* (Figure 5B), and the binding increased *ACS2^W* protein levels by approximately 37% in this system (Figure 5C). Gel-shift assay results demonstrated that YTH1 has a higher binding affinity for the methylated *ACS2^{1287C}* probe compared with the unmethylated *ACS2^{1287C}* probe, and the synonymous mutation completely eliminated the affinity of YTH1 for *ACS2^{1287T}* probe (Figures S5D and S5E). We noted that the 1287C>T synonymous SNP occurred in the UGAC/TA context, which closely resembles an m^{6}A consensus motif (DRACH), and then additional synonymous mutations, changing T^{1284} or T^{1296} into C, were designed to investigate the function of the synonymous SNP in determining enhanced TE of *ACS2* (Figure S5C). The synonymous

Please cite this article in press as: Xin et al., Recessive epistasis of a synonymous mutation confers cucumber domestication through epi-transcriptomic regulation, Cell (2025), https://doi.org/10.1016/j.cell.2025.06.007

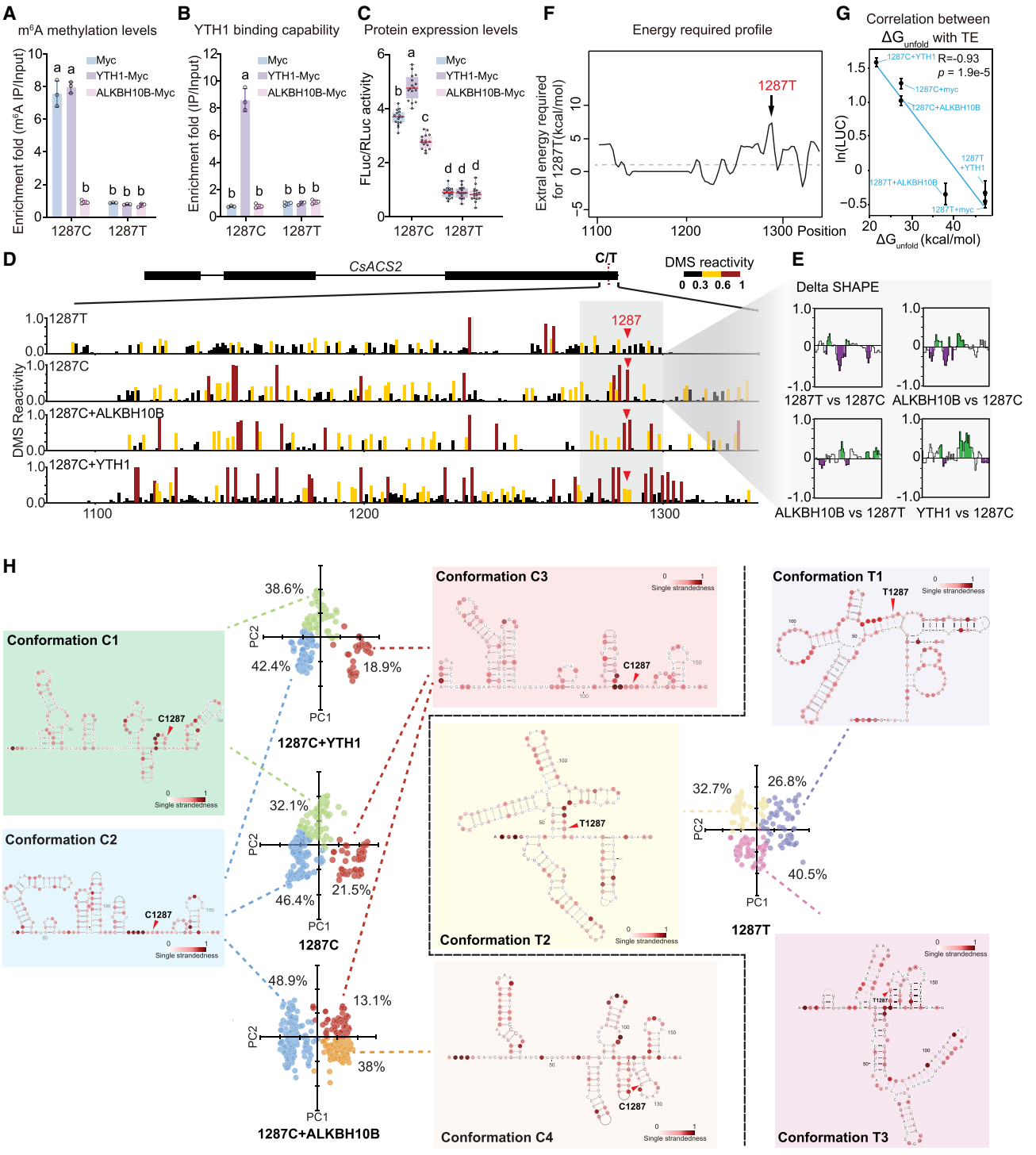

Figure 5. The 1287C>T synonymous mutation changes the TE of *ACS2* via m^{6}A modification and RNA structural alterations

(A) m^{6}A-RIP-qPCR showed the m^{6}A methylation level of *ACS2*^{1287C} and *ACS2*^{1287T} co-expressed with Myc, YTH1-Myc, and ALKBH10B-Myc, respectively. Data are means ± SD. Different letters indicate significant differences ($p < 0.05$, one-way ANOVA and Tukey's test; $n = 3$).

(B) FA-CLIP showed the capability of YTH1^W binding to *ACS2*^{1287C} and *ACS2*^{1287T} co-expressed with Myc, YTH1-Myc, and ALKBH10B-Myc, respectively. Data are means ± SD. Different letters indicate significant differences ($p < 0.05$, one-way ANOVA and Tukey's test; $n = 3$).

(C) Dual-luciferase reporter assays showed the protein levels of *ACS2*^{1287C} and *ACS2*^{1287T} co-expressed with Myc, YTH1-Myc, and ALKBH10B-Myc, respectively. Data are means ± SD. Different letters indicate significant differences ($p < 0.05$, one-way ANOVA and Tukey's test; $n = 16$).

(legend continued on next page)

mutation of 1296T>C outside the DRACH motif had no effect on m^{6}A levels and protein expression levels (Figures S5F–S5H). While similar to the effect of 1287C>T, the 1284T>C also resulted in a complete abolition of m^{6}A modification, YTH1^W binding capacity, and protein expression levels of *ACS2* (Figures S5F–S5H). We also found that the overexpression of *ALKBH10B* significantly reduced the m^{6}A level of *ACS2*^{1287C} to the level of *ACS2*^{1287T} (Figure 5A), and correspondingly almost completely abolished the interaction between YTH1^W and *ACS2*^{1287C} mRNA, but it reduced the protein levels of *ACS2*^{1287C} to a certain extent by 44% (Figures 5A–5C and S5F–S5H). And there was no effect on *ACS2*^{1287T} (Figures 5A–5C). These results indicated that the increased *ACS2* TE determined by the synonymous C^{1287} SNP is partially attributed to the m^{6}A methylation and YTH1^W binding in wild cucumber.

As the reduction in the protein level of *ACS2*^{1287C} when m^{6}A modification was removed was never as pronounced as that observed in the *ACS2*^{1287T} allele (Figure 5C), we then assessed the underlying molecular mechanisms of how the 1287C>T synonymous mutation alters TE. Since folded structures in the coding region of an mRNA act as a kinetic barrier during translation,[8,31,32] we performed *in vivo* RNA structure profiling in cucumber to compare the RNA structures between *ACS2*^{1287T} and *ACS2*^{1287C} alleles.[33,34] Two independent replicates showed high correlations (R = 0.99), allowing us to combine data for downstream analysis (Figure S5I). The *ACS2*^{1287T} allele displayed overall lower dimethyl sulfate (DMS) reactivity, indicating a more compact structure compared with the *ACS2*^{1287C} allele (Figure 5D). Notably, the 1287C>T synonymous mutation exhibited distinct reactivity patterns, with *ACS2*^{1287C} showing significantly high DMS reactivity as the single-strandedness, while *ACS2*^{1287T} showed the double-strandedness. DeltaSHAPE analysis further revealed a significant reduction in DMS reactivity across the 1287C>T synonymous mutation (Figure 5E, $p < 0.001$), indicating that this mutation leads to local significant RNA structure alterations.

Since m^{6}A modification affects RNA structure,[35,36] we then assessed the DMS reactivities of *ACS2*^{1287C} plus *ALKBH10B-Myc* with a significant reduction of m^{6}A level. We found that the DMS reactivities of both the synonymous mutation site and the local flanking regions in the combination of *ACS2*^{1287C} plus *ALKBH10B-Myc* are significantly lower than those of the *ACS2*^{1287C} allele but higher than those of the *ACS2*^{1287T} (Figure 5D). In the expression of *ACS2*^{1287C} plus *YTH1*^{W}*-Myc*, we found that there are significantly higher DMS reactivities across the 1287C>T synonymous mutation site in comparison with those in the *ACS2*^{1287C} allele (Figure 5E). These RNA structural changes were not observed in the combinations of *ACS2*^{1287T} plus *ALKBH10B-Myc* and *ACS2*^{1287T} plus *YTH1*^{W}*-Myc* (Figure S5J).

With observed distinct RNA structural alterations across the 1287C>T synonymous mutation site, we further assessed the impact of these RNA structural changes on TE. We calculated the energy barrier required to unfold the RNA structure per ribosome occupancy window, ΔG_{unfold},[37] across the *ACS2* coding region. We revealed that the *ACS2*^{1287T} allele presents a higher energy barrier (ΔG_{unfold}) across the 1287C>T synonymous mutation site compared with the *ACS2*^{1287C} allele, with an excess of $\Delta G_{unfold} = 7.57$ (Figures 5F and 5G). We further correlated the individual ΔG_{unfold} across the 1287C>T synonymous mutation site with the corresponding TE for *ACS2*^{1287C}, *ACS2*^{1287C} plus *ALKBH10B-Myc*, *ACS2*^{1287C} plus *YTH1*^{W}*-Myc*, *ACS2*^{1287T}, *ACS2*^{1287T} plus *ALKBH10B-Myc*, and *ACS2*^{1287T} plus *YTH1*^{W}*-Myc*. We found a strong correlation between ΔG_{unfold} and TE, suggesting that the energy barrier of unfolding RNA structure determines TE ($R = -0.93$, $p = 1.9 \times 10^{-5}$; Figure 5G). The quantitative associations between ΔG_{unfold} and TE suggest that the increased TE of *ACS2* associated with the C^{1287} synonymous SNP is attributed to both the m^{6}A modifications and the RNA structural changes.

To further investigate the relationship between m^{6}A and RNA structure, we assessed the RNA structural conformation diversity at single-molecule resolution using determination of the variation of the RNA structure conformation through stochastic context-free grammar (DAVINCI).[33] We identified at least three major structural conformations of *ACS2*^{1287C} (32.1% conformation C1; 46.4% conformation C2; 21.5% conformation C3), where all the structural conformations showed single-strandedness across the 1287C>T synonymous mutation site (Figure 5H). In the combination of *ACS2*^{1287C} plus *YTH1*^{W}*-Myc*, these conformations remained largely unchanged, though their proportions slightly shifted (38.6% conformation C1; 42.4% conformation C2; 18.9% conformation C3). Notably, the conformation C1 exhibits the weakest structure, suggesting that YTH1 may shift the folding equilibrium toward the weakest RNA structural conformations. In the combination of *ACS2*^{1287C} plus *ALKBH10B-Myc* with a significant reduction of m^{6}A level, the weakest RNA structural conformation C1 (32.1%) was changed into a more compact RNA structural conformation C4 (38%), with the 1287C>T synonymous mutation site forming into the base pairing along with the proportional changes of the other two conformations (conformation C2 increased to 48.9%, while conformation C3 decreased from

(D) DMS reactivity profile of the *ACS2* alleles. Bar plots showing the DMS reactivity of the indicated region on the *ACS2* locus for the *ACS2*^{1287T}, *ACS2*^{1287C}, and *ACS2*^{1287C} co-expressed with *ALKBH10B* and *YTH1*, respectively. Red triangles showed the position of the 1287 synonymous mutations.

(E) DeltaSHAPE profiles showed DMS reactivity differences in the gray-shaded region from (D), calculated as the difference between each first and latter condition: *ACS2*^{1287T} vs. *ACS2*^{1287C} (1287T vs. 1287C), *ACS2*^{1287C} co-expressed with ALKBH10B vs. *ACS2*^{1287C} (ALKBH10B vs. 1287C), *ACS2*^{1287C} co-expressed with YTH1 vs. *ACS2*^{1287C} (YTH1 vs. 1287C), and *ACS2*^{1287C} co-expressed with ALKBH10B vs. *ACS2*^{1287T} (ALKBH10B vs. 1287T), respectively. Nucleotides colored green indicate significantly increased DMS reactivity, while those in purple indicate significantly decreased DMS reactivity.

(F) The difference in energy required to open up the RNA structure between the *ACS2*^{1287T} and *ACS2*^{1287C} alleles. The position of the synonymous mutation is indicated with a black arrow. Gray dotted lines are the baseline of energy.

(G) Pearson correlation between TE from (C) with their corresponding ΔG_{unfold}. p value was calculated using a two-sided t test. +, plus.

(H) Representative structural models of conformations in *ACS2*^{1287T}, *ACS2*^{1287C}, and *ACS2*^{1287C} co-expressed with *ALKBH10B* or *YTH1*, respectively. Structures were visualized using principal-component analysis (PCA).

See also Figure S5.

21.5% to 13.1%) (Figure 5H). These results indicated that the loss of m^{6}A promotes base pairing across the synonymous mutation and shifts the folding equilibrium toward more stable RNA structural conformations. Thus, m^{6}A affects both the proportion and conformation of RNA structures in *ACS2*^{1287C}. Interestingly, the *ACS2*^{1287T} allele displayed three distinct major RNA structural conformations with much more compact structures than those in the *ACS2*^{1287C} (Figure 5H), suggesting that the 1287C>T synonymous mutation significantly alters RNA structural conformation diversity of *ACS2*.

In summary, we proposed that in developing fruit of wild species, the C^{1287} synonymous SNP results in the m^{6}A modification on nearby adenosine residues and the formation of loose RNA secondary structural conformations in transcripts of the wild *ACS2* allele, thereby facilitating its protein expression. The closely linked *YTH1*^{W} preferentially binds to the m^{6}A modification, shifts the folding equilibrium toward the weakest RNA structural conformation, and further promotes the *ACS2* TE. This leads to increased ethylene production and reduced cell division, contributing to shorter fruit in wild cucumbers. This regulatory module was disrupted in modern cultivars by the T^{1287} synonymous mutation through the impairment in m^{6}A methylation and the formation of compact RNA structural conformations during domestication, leading to attenuated protein production and fruit elongation.

DISCUSSION

Synonymous mutations are known to influence several cellular processes, but there is a shortage of genetic evidence or insights into the underlying regulatory mechanism. Our finding, in this study, highlights a key role of synonymous mutations in determining complex traits and the need for further research into the effects of synonymous mutations on genetic and molecular processes.

As synonymous changes are more common in closely related species than non-synonymous mutations, the longstanding view holds that they may predominantly result in neutral variants.[38–41] Recently, a large-scale phylogenomic analysis of members of the Solanaceae revealed that 15% of 367,499 deleterious variants are synonymous mutations, which is only second to non-synonymous mutations, suggesting that some synonymous SNPs are functionally important and have been selected for during evolution.[6] *ACS2* plays a crucial role in sex determination and ovary development, and loss of *ACS2* function caused by non-synonymous mutations results in andromonoecious, or hermaphrodite, cucurbit crops,[42] which would impair their fitness in many settings under natural selection. While fruit length variation affected by the 1287C>T synonymous mutation does not affect sex determination and might be consistently neutral, so that it can persist during evolution. These findings suggest that synonymous mutations could be selected during domestication to alter post-transcriptional gene expression, such as TE, in response to selective pressures. This challenges the traditional view and highlights the potential importance of synonymous mutations in crop improvement strategies.

A recent study found that a category of synonymous mutations can perturb m^{6}A modification patterns and promote tumorigenesis through mRNA expression regulation.[43] Our work here suggests that in plants, synonymous mutation exploits RNA m^{6}A methylation and RNA structure as action modes to regulate ACS2 TE for fruit domestication. Previous studies have shown that m^{6}A modification affects RNA structures.[35,36] However, these studies were based on the ensemble RNA structures, which represent an average of all the RNA structural conformations.[35,36,44,45] In this study, the use of the single-molecule *in vivo* RNA structure profiling method enabled the determination of the *ACS2*^{C1287} RNA structural diversity (Figure 5H). The loss of m^{6}A not only promotes the formation of stronger structural conformations but also tunes the folding equilibrium toward more stable RNA structural conformations (Figure 5H). Given the strong impact of m^{6}A modification on RNA structural diversity in *ACS2*^{1287C}, the level of m^{6}A may be underestimated due to limitations in current detection methods for low-abundance, cell-type-specific mRNAs like *ACS2*. Furthermore, YTH1 serves as a fine tuner in shifting the folding equilibrium of the RNA structural conformations. Therefore, with the single-molecule resolution of RNA structural information, we were able to capture the changes of the complete RNA structural diversity *in vivo* and revealed how m^{6}A modifications shape the RNA structural diversity.

Although this single synonymous mutation confers fruit length domestication through both m^{6}A modification and RNA structure-mediated mechanisms, the observed significant fruit elongation caused by *YTH1* knockout under the *ACS2*^{W} background (disrupted YTH1's interaction with m^{6}A modification) indicated that genetically the effect of m^{6}A modification substantially contributes to the complex trait. Direct genetic links between mRNA m^{6}A methylation and naturally evolved traits have not been widely reported. Recent work mined the genetic loci that determine m^{6}A levels via the m^{6}A QTL, providing evidence for the role of m^{6}A variants in the heritability of human disease.[46] Given the diverse roles of m^{6}A, the integration of synonymous mutations in the analysis of QTLs for m^{6}A levels may lead to other significant discoveries connecting m^{6}A methylation with other plant properties. Additionally, artificial synonymous *ACS2* mutation at 1284T>C mimicked the effect of the 1287C>T mutation (Figures S5F–S5H), presenting a potential way to specifically reverse m^{6}A modification by direct manipulation of DNA sequences through CRISPR-based systems without changing the encoded amino acids.

Recent research highlighted the critical roles of RNA demethylation in controlling plant growth and seed yield.[47] Further research into the role of synonymous mutations in RNA modification and structure could provide valuable insights for breeding programs, offering potential ways for crop engineering in the future.

Limitations of the study

Due to the lack of effective adenine base editing (ABE) tools that do not rely on NGG protospacer-adjacent motif (PAM) sequence in cucumber, we currently are unable to directly install the m^{6}A modification in *ACS2*^{C} by targeting the synonymous mutation T^{1287} to C. Future genome editing tool development may help create variations at the m^{6}A site with precision. Due to inherent limitations of Ribo-seq methods—specifically the low expression levels of *ACS2* and the position of the 1287C>T

synonymous SNP near the 3′ end of the CDS where ribosome density is typically low—we were unable to obtain sufficient read coverage to assess codon-level ribosome occupancy. As a result, we could not compare A-site ribosome occupancy at the synonymous SNP between the *ACS2*^{1287T} and *ACS2*^{1287C}, and therefore, the other possible regulatory mechanism of the synonymous SNP determining protein level could not be completely ruled out. Future advances in hypersensitive ribosome profiling technologies may enable deeper exploration of this translational dynamics.

RESOURCE AVAILABILITY

Lead contact

Further information and requests for resources and reagents should be directed to, and will be fulfilled by, the lead contact, Xueyong Yang (yangxueyong@caas.cn).

Materials availability

Materials generated in this study are available from the lead contact with a completed materials transfer agreement.

Data and code availability

- Sequencing data have been deposited to the Genome Sequence Archive (GSA; https://ngdc.cncb.ac.cn/gsa/) at the Beijing Institute of Genomics (BIG) Data Center, Chinese Academy of Sciences, under accession number PRJCA037804.
- This paper does not report original code.
- Any additional information required to reanalyze the data reported in this paper is available from the lead contact upon request.

ACKNOWLEDGMENTS

We thank Mr. Zhaonian Dong from the Agricultural Genomics Institute at Shenzhen and Dr. Hongjia Xin from the Institute of Vegetables and Flowers, Chinese Academy of Agricultural Sciences, for helping with bioinformatic analysis. We also thank Prof. Xiaofeng Cao from the Institute of Genetics and Developmental Biology, Chinese Academy of Sciences, for critical comments on this work. C.H. is a Howard Hughes Medical Institute investigator. This work was financially supported by the National Natural Science Foundation of China (NSFC) (grants 31922076 to X.Y. and 31530066 to S.H.); the National Key Research and Development Program of China (2021YFF1000102); the Science and Technology Innovation Program of the Chinese Academy of Agricultural Sciences (CAAS-ASTIP); the special funds for science technology innovation and industrial development of Shenzhen Dapeng New District (grant no. PT202101-17); the Key-Area Research and Development Program of Guangdong Province (2018B020202007 to S.H.); the Shenzhen Peacock Plan (KQTD2016113010482651); the Science, Technology, and Innovation Commission of Shenzhen Municipality (no. ZDSYS20200811142605017); the European Research Council (ERC) selected by the ERC, funded by BBSRC Horizon Europe Guarantee (grant no. EP/Y009886/1); and the United Kingdom Biotechnology and Biological Science Research Council (BBSRC) (grant no. BB/X01102X/1). We thank PlantScribe (www.plantscribe.com) for editing this manuscript.

AUTHOR CONTRIBUTIONS

S.H. and X.Y. conceived the project. X.Y., S.H., and Y.D. designed the study. T.X. and Zhen Zhang made major contributions to biochemical analysis assays and genetic analysis. X.L. contributed to protein purification and FL-CLIP assays. Y.Z. contributed to the mRNA structure analysis. G.W. and H.L. contributed to the detection of m^{6}A at single-base resolution. W.T. and Y.-L.X. contributed to the purification of TadA8.20. T.X. and X.Y. contributed to the genetic transformation of cucumber. S.W. helped design molecular assays. T.X., X.L., and H.T. performed plant phenotype analyses. S.W. helped collect materials and construct vectors. M.Z. and Zhonghua Zhang led the bioinformatic analyses. X.Y. and S.H. composed the outline of the manuscript with input from all authors. X.Y., S.H., T.X., Y.D., and Y.Z. analyzed the data and wrote the manuscript. C.H. edited the manuscript and provided valuable discussion.

DECLARATION OF INTERESTS

S.H. is a member of the *Cell* advisory board.

STAR★METHODS

Detailed methods are provided in the online version of this paper and include the following:

- KEY RESOURCES TABLE
- EXPERIMENTAL MODEL AND SUBJECT DETAILS
  - Plant materials and growth conditions
- METHOD DETAILS
  - QTL analysis and fine mapping of the *FL1.1* and *FL1.2* loci
  - Identification of domestication sweeps
  - Calculation of cell size and number
  - Plasmid construction
  - qRT-PCR Analysis
  - Immunoblotting analysis
  - Transient expression and dual-luciferase assays in cucumber cotyledons
  - Cucumber genetic transformation
  - Southern blot
  - Subcellular localization of YTH1
  - *In situ* hybridization
  - FA-CLIP
  - m^{6}A-seq and m^{6}A-RIP-qPCR
  - eTAM seq and site-specification amplification
  - ALKBH10B-associated SELECT for detection of m^{6}A
  - Absolute quantification of m^{6}A modification
  - Ribosome profiling
  - Ethylene release measurement
  - RNA electrophoretic mobility shift
  - *In vivo* smStructure-seq library construction
  - smStructure-seq data analysis
  - Calculation of ΔG_{unfold}
  - Structural analysis by DaVinci
- QUANTIFICATION AND STATISTICAL ANALYSIS

SUPPLEMENTAL INFORMATION

Supplemental information can be found online at https://doi.org/10.1016/j.cell.2025.06.007.

Received: August 24, 2022
Revised: March 31, 2025
Accepted: June 6, 2025
Corrected online: July 8, 2025

REFERENCES

1. Dhindsa, R.S., Wang, Q., Vitsios, D., Burren, O.S., Hu, F., DiCarlo, J.E., Kruglyak, L., MacArthur, D.G., Hurles, M.E., and Petrovski, S. (2022). A minimal role for synonymous variation in human disease. Am. J. Hum. Genet. *109*, 2105–2109. https://doi.org/10.1016/j.ajhg.2022.10.016.
2. Poon, G.Y., Watson, C.J., Fisher, D.S., and Blundell, J.R. (2021). Synonymous mutations reveal genome-wide levels of positive selection in healthy tissues. Nat. Genet. *53*, 1597–1605. https://doi.org/10.1038/s41588-021-00957-1.

3. Supek, F., Miñana, B., Valcárcel, J., Gabaldón, T., and Lehner, B. (2014). Synonymous mutations frequently act as driver mutations in human cancers. Cell *156*, 1324–1335. https://doi.org/10.1016/j.cell.2014.01.051.

4. Shen, X., Song, S., Li, C., and Zhang, J. (2022). Synonymous mutations in representative yeast genes are mostly strongly non-neutral. Nature *606*, 725–731. https://doi.org/10.1038/s41586-022-04823-w.

5. Kruglyak, L., Beyer, A., Bloom, J.S., Grossbach, J., Lieberman, T.D., Mancuso, C.P., Rich, M.S., Sherlock, G., and Kaplan, C.D. (2023). Insufficient evidence for non-neutrality of synonymous mutations. Nature *616*, E8–E9. https://doi.org/10.1038/s41586-023-05865-4.

6. Wu, Y., Li, D., Hu, Y., Li, H., Ramstein, G.P., Zhou, S., Zhang, X., Bao, Z., Zhang, Y., Song, B., et al. (2023). Phylogenomic discovery of deleterious mutations facilitates hybrid potato breeding. Cell *186*, 2313–2328.e15. https://doi.org/10.1016/j.cell.2023.04.008.

7. Presnyak, V., Alhusaini, N., Chen, Y.H., Martin, S., Morris, N., Kline, N., Olson, S., Weinberg, D., Baker, K.E., Graveley, B.R., et al. (2015). Codon optimality is a major determinant of mRNA stability. Cell *160*, 1111–1124. https://doi.org/10.1016/j.cell.2015.02.029.

8. Gaither, J.B., Lammi, G.E., Li, J.L., Gordon, D.M., Kuck, H.C., Kelly, B.J., Fitch, J.R., and White, P. (2021). Synonymous variants that disrupt messenger RNA structure are significantly constrained in the human population. GigaScience *10*, giab023. https://doi.org/10.1093/gigascience/giab023.

9. Hunt, R.C., Simhadri, V.L., Iandoli, M., Sauna, Z.E., and Kimchi-Sarfaty, C. (2014). Exposing synonymous mutations. Trends Genet. *30*, 308–321. https://doi.org/10.1016/j.tig.2014.04.006.

10. Wan, Y., Qu, K., Zhang, Q.C., Flynn, R.A., Manor, O., Ouyang, Z., Zhang, J., Spitale, R.C., Snyder, M.P., Segal, E., et al. (2014). Landscape and variation of RNA secondary structure across the human transcriptome. Nature *505*, 706–709. https://doi.org/10.1038/nature12946.

11. Lackey, L., Coria, A., Woods, C., McArthur, E., and Laederach, A. (2018). Allele-specific SHAPE-MaP assessment of the effects of somatic variation and protein binding on mRNA structure. Rna *24*, 513–528. https://doi.org/10.1261/rna.064469.117.

12. Roundtree, I.A., Evans, M.E., Pan, T., and He, C. (2017). Dynamic RNA Modifications in Gene Expression Regulation. Cell *169*, 1187–1200. https://doi.org/10.1016/j.cell.2017.05.045.

13. Dominissini, D., Moshitch-Moshkovitz, S., Schwartz, S., Salmon-Divon, M., Ungar, L., Osenberg, S., Cesarkas, K., Jacob-Hirsch, J., Amariglio, N., Kupiec, M., et al. (2012). Topology of the human and mouse m^6A RNA methylomes revealed by m^6A-seq. Nature *485*, 201–206. https://doi.org/10.1038/nature11112.

14. Meyer, K.D., Saletore, Y., Zumbo, P., Elemento, O., Mason, C.E., and Jaffrey, S.R. (2012). Comprehensive analysis of mRNA methylation reveals enrichment in 3′ UTRs and near stop codons. Cell *149*, 1635–1646. https://doi.org/10.1016/j.cell.2012.05.003.

15. Wang, X., Lu, Z., Gomez, A., Hon, G.C., Yue, Y., Han, D., Fu, Y., Parisien, M., Dai, Q., Jia, G., et al. (2014). N^6-methyladenosine-dependent regulation of messenger RNA stability. Nature *505*, 117–120. https://doi.org/10.1038/nature12730.

16. Wang, X., Zhao, B.S., Roundtree, I.A., Lu, Z., Han, D., Ma, H., Weng, X., Chen, K., Shi, H., and He, C. (2015). N^6-methyladenosine Modulates Messenger RNA Translation Efficiency. Cell *161*, 1388–1399. https://doi.org/10.1016/j.cell.2015.05.014.

17. Wang, X., and He, C. (2014). Reading RNA methylation codes through methyl-specific binding proteins. RNA Biol. *11*, 669–672. https://doi.org/10.4161/rna.28829.

18. Fu, Y., Jia, G., Pang, X., Wang, R.N., Wang, X., Li, C.J., Smemo, S., Dai, Q., Bailey, K.A., Nobrega, M.A., et al. (2013). FTO-mediated formation of N^6-hydroxymethyladenosine and N^6-formyladenosine in mammalian RNA. Nat. Commun. *4*, 1798. https://doi.org/10.1038/ncomms2822.

19. Jia, G., Fu, Y., Zhao, X., Dai, Q., Zheng, G., Yang, Y., Yi, C., Lindahl, T., Pan, T., Yang, Y.-G., et al. (2011). N^6-methyladenosine in nuclear RNA is a major substrate of the obesity-associated FTO. Nat. Chem. Biol. *7*, 885–887. https://doi.org/10.1038/nchembio.687.

20. Duan, H.-C., Wei, L.-H., Zhang, C., Wang, Y., Chen, L., Lu, Z., Chen, P.R., He, C., and Jia, G. (2017). ALKBH10B is an RNA N^6-methyladenosine demethylase affecting Arabidopsis floral transition. Plant Cell *29*, 2995–3011. https://doi.org/10.1105/tpc.16.00912.

21. Zheng, G., Dahl, J.A., Niu, Y., Fedorcsak, P., Huang, C.-M., Li, C.J., Vågbø, C.B., Shi, Y., Wang, W.-L., Song, S.-H., et al. (2013). ALKBH5 is a mammalian RNA demethylase that impacts RNA metabolism and mouse fertility. Mol. Cell *49*, 18–29. https://doi.org/10.1016/j.molcel.2012.10.015.

22. Liu, N., Dai, Q., Zheng, G., He, C., Parisien, M., and Pan, T. (2015). N^6-methyladenosine-dependent RNA structural switches regulate RNA–protein interactions. Nature *518*, 560–564. https://doi.org/10.1038/nature14234.

23. Liu, N., Zhou, K.I., Parisien, M., Dai, Q., Diatchenko, L., and Pan, T. (2017). N^6-methyladenosine alters RNA structure to regulate binding of a low-complexity protein. Nucleic Acids Res. *45*, 6051–6063. https://doi.org/10.1093/nar/gkx141.

24. Qi, J., Liu, X., Shen, D., Miao, H., Xie, B., Li, X., Zeng, P., Wang, S., Shang, Y., Gu, X., et al. (2013). A genomic variation map provides insights into the genetic basis of cucumber domestication and diversity. Nat. Genet. *45*, 1510–1515. https://doi.org/10.1038/ng.2801.

25. Xin, T., Zhang, Z., Li, S., Zhang, S., Li, Q., Zhang, Z.-H., Huang, S., and Yang, X. (2019). Genetic regulation of ethylene dosage for cucumber fruit elongation. Plant Cell *31*, 1063–1076. https://doi.org/10.1105/tpc.18.00957.

26. Wei, L.-H., Song, P., Wang, Y., Lu, Z., Tang, Q., Yu, Q., Xiao, Y., Zhang, X., Duan, H.-C., and Jia, G. (2018). The m^6A reader ECT2 controls trichome morphology by affecting mRNA stability in Arabidopsis. Plant Cell *30*, 968–985. https://doi.org/10.1105/tpc.17.00934.

27. Xiao, Y.L., Liu, S., Ge, R., Wu, Y., He, C., Chen, M., and Tang, W. (2023). Transcriptome-wide profiling and quantification of N^6-methyladenosine by enzyme-assisted adenosine deamination. Nat. Biotechnol. *41*, 993–1003. https://doi.org/10.1038/s41587-022-01587-6.

28. Xiao, Y., Wang, Y., Tang, Q., Wei, L., Zhang, X., and Jia, G. (2018). An elongation-and ligation-based qPCR amplification method for the radiolabeling-free detection of locus-Specific N^6-methyladenosine modification. Angew. Chem. Int. Ed. Engl. *57*, 15995–16000. https://doi.org/10.1002/anie.201807942.

29. Wan, W., Ao, X., Chen, Q., Yu, Y., Ao, L., Xing, W., Guo, W., Wu, X., Pu, C., Hu, X., et al. (2022). METTL3/IGF2BP3 axis inhibits tumor immune surveillance by upregulating N^6-methyladenosine modification of PD-L1 mRNA in breast cancer. Mol. Cancer *21*, 60. https://doi.org/10.1186/s12943-021-01447-y.

30. Han, D., Liu, J., Chen, C., Dong, L., Liu, Y., Chang, R., Huang, X., Liu, Y., Wang, J., Dougherty, U., et al. (2019). Anti-tumour immunity controlled through mRNA m^6A methylation and YTHDF1 in dendritic cells. Nature *566*, 270–274. https://doi.org/10.1038/s41586-019-0916-x.

31. Qu, X.H., Wen, J.D., Lancaster, L., Noller, H.F., Bustamante, C., and Tinoco, I. (2011). The ribosome uses two active mechanisms to unwind messenger RNA during translation. Nature *475*, 118–121. https://doi.org/10.1038/nature10126.

32. Wen, J.D., Lancaster, L., Hodges, C., Zeri, A.C., Yoshimura, S.H., Noller, H.F., Bustamante, C., and Tinoco, I. (2008). Following translation by single ribosomes one codon at a time. Nature *452*, 598–603. https://doi.org/10.1038/nature06716.

33. Yang, M., Zhu, P., Cheema, J., Bloomer, R., Mikulski, P., Liu, Q., Zhang, Y., Dean, C., and Ding, Y. (2022). In vivo single-molecule analysis reveals COOLAIR RNA structural diversity. Nature *609*, 394–399. https://doi.org/10.1038/s41586-022-05135-9.

34. Bohn, P., Gribling-Burrer, A.S., Ambi, U.B., and Smyth, R.P. (2023). Nano-DMS-MaP allows isoform-specific RNA structure determination. Nat. Methods *20*, 849–859. https://doi.org/10.1038/s41592-023-01862-7.

35. Höfler, S., and Duss, O. (2024). Interconnections between m^{6}A RNA modification, RNA structure, and protein–RNA complex assembly. Life Sci. Alliance *7*, e202302240. https://doi.org/10.26508/lsa.202302240.

36. Roost, C., Lynch, S.R., Batista, P.J., Qu, K., Chang, H.Y., and Kool, E.T. (2015). Structure and thermodynamics of N^6-methyladenosine in RNA: a spring-loaded base modification. J. Am. Chem. Soc. *137*, 2107–2115. https://doi.org/10.1021/ja513080v.

37. Mustoe, A.M., Busan, S., Rice, G.M., Hajdin, C.E., Peterson, B.K., Ruda, V. M., Kubica, N., Nutiu, R., Baryza, J.L., and Weeks, K.M. (2018). Pervasive Regulatory Functions of mRNA Structure Revealed by High-Resolution SHAPE Probing. Cell *173*, 181–195.e18. https://doi.org/10.1016/j.cell.2018.02.034.

38. Graur, D., Sater, A.K., and Cooper, T.F. (2016). MOL BIOL EVOL (Springer).

39. Kimura, M. (1968). Genetic variability maintained in a finite population due to mutational production of neutral and nearly neutral isoalleles. Genet. Res. *11*, 247–269. https://doi.org/10.1017/s0016672300011459.

40. Nei, M., and Kumar, S. (2000). Molecular Evolution and Phylogenetics (Oxford University Press) https://doi.org/10.1093/oso/9780195135848.001.0001.

41. Richmond, R.C. (1970). Non-Darwinian evolution: a critique. Nature *225*, 1025–1028. https://doi.org/10.1038/2251025a0.

42. Zhang, S., Tan, F.Q., Chung, C.H., Slavkovic, F., Devani, R.S., Troadec, C., Marcel, F., Morin, H., Camps, C., Gomez Roldan, M.V., et al. (2022). The control of carpel determinacy pathway leads to sex determination in cucurbits. Science *378*, 543–549. https://doi.org/10.1126/science.add4250.

43. Lan, Y., Xia, Z., Shao, Q., Lin, P., Lu, J., Xiao, X., Zheng, M., Chen, D., Dou, Y., and Xie, Q. (2025). Synonymous mutations promote tumorigenesis by disrupting m^{6}A-dependent mRNA metabolism. Cell *188*, 1828–1841.e15. https://doi.org/10.1016/j.cell.2025.01.026.

44. Micura, R., Pils, W., Höbartner, C., Grubmayr, K., Ebert, M.O., and Jaun, B. (2001). Methylation of the nucleobases in RNA oligonucleotides mediates duplex–hairpin conversion. Nucleic Acids Res. *29*, 3997–4005. https://doi.org/10.1093/nar/29.19.3997.

45. Engel, J.D., and von Hippel, P.H. (1978). Effects of methylation on the stability of nucleic acid conformations. Studies at the polymer level. J. Biol. Chem. *253*, 927–934. https://doi.org/10.1021/bi00717a013.

46. Zhang, Z., Luo, K., Zou, Z., Qiu, M., Tian, J., Sieh, L., Shi, H., Zou, Y., Wang, G., Morrison, J., et al. (2020). Genetic analyses support the contribution of mRNA N^6-methyladenosine (m^{6}A) modification to human disease heritability. Nat. Genet. *52*, 939–949. https://doi.org/10.1038/s41588-020-0644-z.

47. Yu, Q., Liu, S., Yu, L., Xiao, Y., Zhang, S., Wang, X., Xu, Y., Yu, H., Li, Y., Yang, J., et al. (2021). RNA demethylation increases the yield and biomass of rice and potato plants in field trials. Nat. Biotechnol. *39*, 1581–1588. https://doi.org/10.1038/s41587-021-00982-9.

48. Dobin, A., Davis, C.A., Schlesinger, F., Drenkow, J., Zaleski, C., Jha, S., Batut, P., Chaisson, M., and Gingeras, T.R. (2013). STAR: ultrafast universal RNA-seq aligner. Bioinformatics *29*, 15–21. https://doi.org/10.1093/bioinformatics/bts635.

49. Zhang, Y., Liu, T., Meyer, C.A., Eeckhoute, J., Johnson, D.S., Bernstein, B. E., Nusbaum, C., Myers, R.M., Brown, M., Li, W., et al. (2008). Model-based analysis of ChIP-Seq (MACS). Genome Biol. *9*, R137. https://doi.org/10.1186/gb-2008-9-9-r137.

50. Tripathi, S., Pohl, M.O., Zhou, Y., Rodriguez-Frandsen, A., Wang, G., Stein, D.A., Moulton, H.M., DeJesus, P., Che, J., Mulder, L.C., et al. (2015). Meta- and Orthogonal Integration of Influenza "OMICs" Data Defines a Role for UBR4 in Virus Budding. Cell Host Microbe *18*, 723–735. https://doi.org/10.1016/j.chom.2015.11.002.

51. Li, H., Handsaker, B., Wysoker, A., Fennell, T., Ruan, J., Homer, N., Marth, G., Abecasis, G., and Durbin, R.; 1000 Genome Project Data Processing Subgroup (2009). The Sequence Alignment/Map format and SAMtools. Bioinformatics *25*, 2078–2079. https://doi.org/10.1093/bioinformatics/btp352.

52. Lorenz, R., Bernhart, S.H., Höner Zu Siederdissen, C., Tafer, H., Flamm, C., Stadler, P.F., and Hofacker, I.L. (2011). ViennaRNA Package 2.0. Algorithms Mol. Biol. *6*, 26. https://doi.org/10.1186/1748-7188-6-26.

53. Thiel, B.C., Beckmann, I.K., Kerpedjiev, P., and Hofacker, I.L. (2019). 3D based on 2D: calculating helix angles and stacking patterns using forgi 2.0, an RNA Python library centered on secondary structure elements. F1000Res *8*, ISCBCommJ-287. https://doi.org/10.12688/f1000research.18458.2.

54. Li, H. (2018). Minimap2: pairwise alignment for nucleotide sequences. Bioinformatics *34*, 3094–3100. https://doi.org/10.1093/bioinformatics/bty191.

55. Smola, M.J., Calabrese, J.M., and Weeks, K.M. (2015). Detection of RNA-Protein Interactions in Living Cells with SHAPE. Biochemistry *54*, 6867–6875. https://doi.org/10.1021/acs.biochem.5b00977.

56. Zong, Y., Song, Q., Li, C., Jin, S., Zhang, D., Wang, Y., Qiu, J.L., and Gao, C. (2018). Efficient C-to-T base editing in plants using a fusion of nCas9 and human APOBEC3A. Nat. Biotechnol. *36*, 950–953. https://doi.org/10.1038/nbt.4261.

57. Xin, T., Tian, H., Ma, Y., Wang, S., Yang, L., Li, X., Zhang, M., Chen, C., Wang, H., and Li, H. (2022). Targeted creation of new mutants with compact plant architecture using CRISPR/Cas9 genome editing by an optimized genetic transformation procedure in cucurbit plants. Hortic. *9*, uhab086. https://doi.org/10.1093/hr/uhab086.

58. Zhang, H., Li, S., Yang, L., Cai, G., Chen, H., Gao, D., Lin, T., Cui, Q., Wang, D., Li, Z., et al. (2021). Gain-of-function of the 1-aminocyclopropane-1-carboxylate synthase gene ACS1G induces female flower development in cucumber gynoecy. Plant Cell *33*, 306–321. https://doi.org/10.1093/plcell/koaa018.

59. Ingolia, N.T., Brar, G.A., Rouskin, S., McGeachy, A.M., and Weissman, J. S. (2012). The ribosome profiling strategy for monitoring translation in vivo by deep sequencing of ribosome-protected mRNA fragments. Nat. Protoc. *7*, 1534–1550. https://doi.org/10.1038/nprot.2012.086.

60. Ingolia, N.T., Lareau, L.F., and Weissman, J.S. (2011). Ribosome profiling of mouse embryonic stem cells reveals the complexity and dynamics of mammalian proteomes. Cell *147*, 789–802. https://doi.org/10.1016/j.cell.2011.10.002.

61. Deigan, K.E., Li, T.W., Mathews, D.H., and Weeks, K.M. (2009). Accurate SHAPE-directed RNA structure determination. Proc. Natl. Acad. Sci. USA *106*, 97–102. https://doi.org/10.1073/pnas.0806929106.

62. Do, C.B., Woods, D.A., and Batzoglou, S. (2006). CONTRAfold: RNA secondary structure prediction without physics-based models. Bioinformatics *22*, e90–e98. https://doi.org/10.1093/bioinformatics/btl246.

Please cite this article in press as: Xin et al., Recessive epistasis of a synonymous mutation confers cucumber domestication through epi-transcriptomic regulation, Cell (2025), https://doi.org/10.1016/j.cell.2025.06.007

STAR★METHODS

KEY RESOURCES TABLE

REAGENT or RESOURCE	SOURCE	IDENTIFIER
Antibodies		
Rabbit Monoclonal Anti-ACS2	Xin et al.[25]	N/A
Mouse Monoclonal Anti-Myc	MBL	Cat# M192-3; RRID:AB_11160947
Rabbit polyclonal Anti-m^{6}A	Synaptic Systems	Cat# 202003; RRID:AB_2279214
Mouse Monoclonal Anti-Actin	Thermo Fisher	Cat# MA5-11869; RRID:AB_11004139
Bacterial and virus strains		
EHA105 Chemically Competent Cells	Weidi Biotechnology Co., Ltd	Cat# AC1010
GV3101 Chemically Competent Cells	Weidi Biotechnology Co., Ltd	Cat# AC1003
E. coli DH5α Chemically Competent Cells	Weidi Biotechnology Co., Ltd	Cat#: DL1001
Biological samples		
DNA and leaf tissue from the CRISPR lines	This study	N/A
DNA and leaf tissue from the transgenic lines	This study	N/A
Chemicals, peptides, and recombinant proteins		
KOD One PCR Master Mix	Toyobo Inc. (Osaka, Japan)	Cat# KMM-201
T4 DNA Ligase	New England Biolabs	Cat# M0202L
Acetosyringone	Sigma	Cat# D134406
HEPES	Millipore Sigma	Cat# 83264
PMSF	Beyotime	Cat# ST506
Proteinase K	Invitrogen	Cat# 25530015
DNase I	New England Biolabs	Cat# M0303
Paraffin	Leica	Cat# 3801360
TRIzol reagent	Invitrogen	Cat#15596018CN
Protease Inhibitor Cocktail	Roche	Cat#11836170001
MES	Sigma	Cat# M8250
Ribonucleoside vanadyl complexes	Sigma	Cat# R3380
β-mercaptoethanol	Gibco	Cat#21985023
N^6-Methyladenosine,5'-monophosphate sodium salt	Sigma	Cat# M2780
*Bsa*I	NEB	Cat# R0535L
*Bam*HI	NEB	Cat# R3136
*Sac*II	NEB	Cat# R0157S
L-ascorbic acid	Sigma	Cat# A92092
α-KG	Apexbio	Cat# M277-50
$(NH_4)_2Fe(SO_4)_2$	Sigma	Cat# 203505
RNase inhibitor	Thermo Fisher	Cat# EO0381
Bst 2.0 DNA polymerase	NEB	Cat# M0537S
SplintR ligase	NEB	Cat# M0375S
Anti-c-Myc Magnetic Beads	Thermo Fisher	Cat# 88842
Protein A Dynabeads	Thermo Fisher	Cat# 10001D
Critical commercial assays		
Dual-Luciferase® Reporter Assay System	Promega	Cat# E1910
TNT® SP6 high-yield wheat germ expression system	Promega	Cat# L3260
Qubit™ RNA HS Assay Kit	Thermo	Cat# Q32852

(*Continued on next page*)

Please cite this article in press as: Xin et al., Recessive epistasis of a synonymous mutation confers cucumber domestication through epi-transcriptomic regulation, Cell (2025), https://doi.org/10.1016/j.cell.2025.06.007

Continued

REAGENT or RESOURCE	SOURCE	IDENTIFIER
GoTaq® qPCR Master Mix	Promega	Cat# A2790
SuperSignal™ West Femto	Thermo	Cat# 34094
PolyATtract® mRNA Isolation Systems	Promega	Cat# Z3101
Pierce™ BCA Protein Assay Kit	Thermo	Cat# 23225
DNeasy Plant Pro kit	QIAGEN	Cat# 69204
Native Barcoding kit	Oxford Nanoporetech	Cat# NBD-24
Oligonucleotides		
Primers listed in Table S2	BGI (Beijing, China)	N/A
Software and algorithms		
Prism 10	Graphpad software, Inc	https://www.graphpad.com/
Geneious	Bioinformatics software, Inc	https://www.geneious.com; RRID: SCR_010519
Image J	Image processing and analysis software, Inc	https://imagej.nih.gov/ij; RRID:SCR_003070
Primer Premier 5	PCR Primer design software, Inc	http://www.premierbiosoft.com/primerdesign/; RRID: SCR_023946
STAR	Dobin et al.[48]	RRID:SCR_004463
MACS2	Zhang et al.[49]	RRID:SCR_013291
HOMER	Tripathi et al.[50]	RRID:SCR_010881
Bowtie2	John Hopkins University	RRID:SCR_016368
SAMtools	Li et al.[51]	RRID:SCR_002105
Illustrator	Adobe	RRID:SCR_010279
Dorado	ONT oxford	RRID:SCR_025883
Davinci	Yang et al.[33]	https://github.com/DingLab-RNAstructure/smStructure-seq
ViennaRNA package	Lorenz et al.[52]	http://www.tbi.univie.ac.at/RNA
Forgi package	Thiel et al.[53]	https://github.com/ViennaRNA/forgi
Minimap2	Li Heng.[54]	https://github.com/lh3/minimap2/tree/master
Contrafold	Stanford	http://contra.stanford.edu/contrafold/
deltaSHAPE	Smola et al.[55]	https://github.com/Weeks-UNC/deltaSHAPE

EXPERIMENTAL MODEL AND SUBJECT DETAILS

Plant materials and growth conditions

Wild cucumber *C. sativus* var. *hardwickii* and cultivated cucumber Xintaimici were used as the donor and recurrent parents, respectively, to develop the backcross population and the introgression lines (ILs). A core collection of wild and domesticated cucumber accessions from our stocks were used as materials for fruit length analysis. To clone the candidate gene, a BC_3S_4 population was derived from a cross between IL-1-1 and Xintaimici. IL-1-1-1 and IL-1-1-6 were used for fine mapping of *FL1.2* and *FL1.1*, respectively.

Seeds were sterilized with 0.6% sodium hypochlorite solution and germinated on moist filter paper. The germinated seeds were sown in 32-cell plastic flats filled with soil and grown in an artificial climate room for 15 d (25°C day/22°C night), then transplanted to the field. All cucumber plants and transgenic plants were grown in the greenhouse under a natural light regime at the Chinese Academy of Agricultural Sciences. Standard water and fertilization management were performed during growth.

METHOD DETAILS

QTL analysis and fine mapping of the *FL1.1* and *FL1.2* loci

The v2.0 cucumber genome was used for genetic analyses. The QTL analysis was carried out based on the genotypes and fruit length of $F_{2:3}$ populations from crosses between *hardwickii* and Xintaimici. The *FL1* locus was first delimited to a 4.5 cM genomic interval by QTL analysis. To generate enough recombinant plants for fine mapping, nine Kompetitive Allele Specific PCR (KSAP) markers (M1-M9) were employed to genotype a BC_3S_3 population containing 8,000 plants derived from the cross of IL-1-1 with Xintaimici. After 3 years of phenotypic investigation, two interaction intervals *FL1.1* and *FL1.2* were localized to a 278 kb and 586 kb genomic interval between the markers M4 and M5, M7 and M8, respectively. For cloning of *ACS2* and *YTH1*, recombinant events were

generated in the *FL1.2* and *FL1.1* regions by backcrossing IL-1-1-1 and IL-1-1-6 to Xintaimici, respectively. All marker information is listed in Table S1. The gene ID of *ACS2* is *Csa1G580750* in v2.0 genome, and is *CsaV3_1G040170* in v3.0 genome. The gene ID of *YTH1* is *Csa1G538270* in v2.0 genome database: cucurbitgenomics.org/organism/2, and is *CsaV3_1G037380* in v3.0 genome database: cucubitgenomics.org/organism/20.

Identification of domestication sweeps

To detect the regions under domestication sweeps, the diversity ratio (π_W/π_C) and the XP-CLR score were combined as previously described.[24] Three cultivated groups (East Asian groups, Eurasian groups and Xishuangbanna groups) were combined into a single cultivated gene pool to identify the domestication sweeps. The regions with lower levels of polymorphisms in cultivated groups were identified using the diversity ratio (π_W/π_C) by comparing Indian groups to cultivated groups. The top 5% of π_W/π_C ratio with the lower diversity in cultivated groups were considered as domestication regions. The XP-CLR was used to detect the regions under selection in cultivated cucumber. 0.05-cM sliding window with 100 bp steps and the maximum number of SNP in each window was assayed to 200. The top 5% of XP-CLR values were also considered as candidate regions. The overlapped regions between the two methods were selected as domestication sweeps.

Calculation of cell size and number

For histological analyses of $FL1.1^C$ $FL1.2^C$, $FL1.1^W$ $FL1.2^C$, $FL1.1^C$ $FL1.2^W$ and $FL1.1^W$ $FL1.2^W$ cucumber fruits, paraffin sections with three biological replicates were made, and three fruit from each NIL line were collected at different development stages as one biological replicate (-5, -3, 0, 3, 5, 8, and 16 days after anthesis). Samples from the mesocarp of the middle part of each fruit along the longitudinal axis were immediately fixed in formaldehyde-acetic acid-ethanol fixative (FAA; 70% ethanol, formaldehyde, and glacial acetic acid in a volume ratio of 90:5:5). 5 mm tissue cubes were embedded in paraffin, and hematoxylin-eosin was used to stain 8-μm-thick sections cut using a microtome (Leica). The stained sections were imaged and photographed by light microscopy (ZEISS).

ImageJ software was used to calculate the average cell size. 60 cells from three independent fruits were pooled and calculated for one biological replicate. The average cell number was determined by calculating the longitudinal section area (S) of sampled fruits and the average cell size (S'), and the area of the longitudinal section was represented by an ellipse. The area S of the longitudinal section of the fruit was determined using the equation $S= \pi \times \text{length} \times \text{diameter}$. The number of cells (N) in the longitudinal section of the whole fruit was calculated using the equation N=S/S'.

Plasmid construction

For dual-luciferase reporter assays, the UTR, CDS and UTR + CDS fragments from $ACS2^C$ and $ACS2^W$ were amplified via PCR. The fused UTR and/or CDS fragments in different combinations were obtained using fusion PCR. All the fragments were inserted into the pGreenII 0800-Luc vector between the *Bam*HI and *Sac*II sites. The fragments with different synonymous mutation combinations in the *ACS2* CDS were obtained by introducing mutations into primers for fusion PCR amplification and were inserted into the pGreenII 0800-Luc vector between the *Bam*HI and *Sac*II sites. Diagrams of the constructs are shown in Figures 2C and 2D.

For CRISPR-Cas9 experiments, the CRISPR-GE web tool (http://skl.scau.edu.cn) was used to design the gRNA target. To generate a double-stranded DNA fragment of the sgRNA, a 50 μL reaction mix containing 1.5 μL 100 μM forward and reverse primers, 1× NEB buffer and 42 μL distilled water was incubated at 95°C for 5 min, and then the temperature was lowered by 0.1°C /s to a final of 20°C. The sgRNA was cloned into the pBSE402[57] vector digested with *Bsa*I to produce the pBSE402-CR-YTH1 construct.

For complementary vectors 1287C and 1287T, a 2kb promoter region and 1338-bp coding sequence with a T to C mutation at the 1287 position were generated by introducing mutations into primers for fusion PCR. The DNA fragments were cloned into the pCAMBIA1305.4 vector, which was modified from pCAMBIA1300 by introducing a GFP expression cassette to generate the 1287C and 1287T vectors.

For *ACS2* C to T base editing at position 1287, the SpCas9 in the pBSE402 vector was replaced with APOBEC3A (A3A) fused with nCas9(D10A)[56] and renamed pBSE402-A3A. We designed the target for C^{1287} to be within the editing window. The methods of target design and construction were similar to those of CRISPR/Cas9. The primers used for plasmid construction are listed in Table S2.

qRT-PCR Analysis

To analyze the *ACS2* and *YTH1* expression patterns, total RNA from $FL1.1^W$ $FL1.2^C$, $FL1.1^W$ $FL1.2^W$ and $FL1.1^C$ $FL1.2^W$ at different developmental stages (-8, -5, -3, 0, 2 Day after anthesis) was extracted using TRIzol reagent (Invitrogen). Three biological replicates were used, and each biological replicate included five ovaries from independent plants. The cDNA was synthesized using the M-MLV Reverse Transcriptase (Promega), and a 20 μl GoTaq® qPCR Master Mix (Promega) reaction volume as was used for qPCR on an ABI 7900 (Applied Biosystems) machine. Relative gene expression was calculated using the $2^{-\Delta\Delta Ct}$ method, with the *CsActin* gene, *Csa6G484600*, as an internal control. Primers used in this experiment are listed in Table S2.

Immunoblotting analysis

Protein was extracted from the fruits of $FL1.1^W$ $FL1.2^C$, $FL1.1^W$ $FL1.2^W$, *WW*, *WC*, *KW* and *KC* at different developmental stages (-8, -5, -3, 0, 2 DAA) using denaturing buffer (20 mM Tris-HCl with pH = 7.5, 150 mM NaCl, 4 M urea, 5 mM DTT, 10% glycerol, 1 × PMSF and 1× cocktail). Five ovaries from five independent plants as one biological replicate, and three biological replicates

were performed. The samples were incubated for 20 min and centrifuged at 12,000 rpm for 20 min at 4°C. The protein was quantified using Pierce™ BCA Protein Assay Kit (Thermo Scientific), and samples were fractionated by 12% SDS-PAGE and then transferred to PVDF membrane (Millipore) using a trans blotter (Bio-Rad). A rabbit polyclonal ACS2 anti-body, raised as previously described, [25] and anti-actin primary antibody (Thermo, MA5-11869) was used for immunoblotting blot analyses. The signal of the target protein was visualized using SuperSignal™ West Femto (Thermo). The relative protein ratio is relative to the loading control (actin).

Transient expression and dual-luciferase assays in cucumber cotyledons

The constructs for dual-luciferase assays were transformed into *Agrobacterium tumefaciens* strain, GV3101. Single clones were shaken overnight in LB liquid medium, before the cells were resuspended in inoculation buffer containing 10 mM $MgCl_2$, 10 mM MES (pH 5.6) and 200 μM Acetosyringone (Sigma, D134406) to OD_{600} = 1.0. The *Agrobacterium* suspension was infiltrated into the abaxial side of one-week-old cucumber cotyledons using 1 mL syringe after incubation for 2 h at 28°C in the dark. The infiltrated cotyledons were then left in the dark for 12 h, transferred to a culture chamber, and grown under a natural light regime. After 3 days of cultivation, cotyledon samples were harvested and frozen at -80°C.

The collected samples of the same size were powdered in liquid nitrogen and the dual-luciferase reporter assays were performed using the Dual-Luciferase® Reporter Assay System (Promega, E1910). The Firefly and Renilla luciferase activities were measured with a GloMax® 20/20 luminometer (E5311, Promega). The luciferase activity of the different constructs was normalized to Renilla luciferase activity.

Cucumber genetic transformation

Cucumber transformation was performed as previously described.[57] Briefly, *Agrobacterium* (EHA105) carrying a construct was used for transformation. Twenty-four hours after initiating seed germination, the cotyledons were transversely cut in half with a sterilized scalpel, and the hypocotyl was excised. The explants were scratched gently with a micro-brush and sonicated in an Ultrasonic cleaning instrument (KQ-100DV) at 100 W for 30 S. The treated explants were vacuum infiltrated with a 20 mL syringe and transferred for co-culturing in the dark for 3 days. After 3-4 weeks of regeneration, positive plants were visually selected using the GFP fluorescence. The transgenic plants were rooted and confirmed by sequencing. All the primers used for vector construction and transgenic line determination are listed in Table S2.

Southern blot

To detect the copy number of 1284T and 1287C transgenic plants, the genomic DNA was extracted from the leaves using DNeasy Plant Pro kit (QIAGEN, 69204) according to the manufacturer's instructions. 10μg DNA was digested with restriction enzymes *Hin*dIII for about 24h at 37°C and then isolated with an equal volume of phenol: chloroform. The prepared sample was subjected to electrophoresis on 0.7% agarose gel at 25V, 4°C overnight and then transferred to Hybond™-N^+ nylon membrane (Amersham, RPN303B). The DNA probe was designed for the transgenic marker GFP and labelled with Digoxigenin (Roach). The membrane was pre-hybridized with 10 mL Hyb-100 (Roach) at 37°C for 2h, and then hybridized with a DIG-labelled probe overnight at 37°C. The hybridized membrane was incubated with anti-DIG antibodies and then photographed. The primers used are listed in Table S2.

Subcellular localization of YTH1

To determine the subcellular localization of *YTH1*, the *YTH1* coding sequence without the termination codon was cloned and inserted into the pCAMBIA1300-GFP vector between the *Kpn*I and *Xba*I sites to generate *35S::YTH1-GFP* vector. *Agrobacterium tumefaciens* GV3101 carrying the vector were cultured and incubated with infiltration buffer (10 mM $MgCl_2$, 10 mM MES, pH 5.2, and 200 mM AS) before *35S::YTH1-GFP* was mixed with the *NLS-RFP* vector and *P19* and then infiltrated into the leaves of tobacco (*Nicotiana benthamiana*). As a control *35S::GFP* empty vector was mixed with the *NLS-RFP* vector and P19. The leaves were imaged with a laser scanning confocal microscope (LEICA). The primers used are listed in Table S2.

In situ hybridization

A DIG RNA labeling Mix (Roche) was used to synthesize the sense and antisense RNA probes for specific *YTH1* and *ACS2* regions. Cucumber fruits at stage 6-8 from $FL1.1^W$ $FL1.2^W$ were used for *in situ* hybridization, as previously described.[58] In brief, samples were fixed, dehydrated, and infiltrated with Steedman wax. The samples were cut into 10-μm sections using a microtome (Leica). Tissue sections with complete morphology were selected for hybridization with probes and subsequent staining. The images were taken using a light microscope (ZEISS). Primers used for probe synthesis are listed in Table S2.

FA-CLIP

To determine the interaction between $YTH1^W$ and $ACS2^C$ or $ACS2^W$, FA-CLIP was carried out as previously described.[20]

Formaldehyde fixation and cross-linking of samples

The ovaries from stable transgenic plants ($YTH1^W$-*Myc* $ACS2^W$, $YTH1^W$-*Myc* $ACS2^C$, $YTH1^C$-*Myc* $ACS2^W$ and $YTH1^C$-*Myc* $ACS2^C$) and cucumber cotyledons transiently co-expressing ($ACS2^{1287C}$, $ACS2^{1287T}$, $ACS2^{1284C}$ and $ACS2^{1296C}$) with or without YTH1-Myc and ALKBH10B-Myc were fixed with 1% formaldehyde solution under vacuum for 30 min at 4°C. After removing the formaldehyde solution, the crosslinking reaction was quenched with 125 mM glycine solution under vacuum for 5 min. The tissues were washed

3 times with precooled water, and the water on the samples was then removed with paper towels. Two biological replicates were used for FA-CLIP seq and three biological replications were used for FA-CLIP-qPCR. Each sampling and measurement used five to ten ovaries from five independent plants as one biological replicate for stable transgenic plants. And five infiltrated cotyledons from five independent plants were used as one biological replicate for cucumber cotyledons transient expression system.

Immunoprecipitation

4 g of tissue was ground into a fine powder and incubated with lysis buffer (50 mM HEPES, pH = 7.5, 0.5% NP-40 [v/v], 150 mM KCl, 0.5 mM DTT, 2 mM EDTA, 1 × cocktail protease inhibitor (Thermo Scientific), and 40 units/mL RNase inhibitor (Roche) for 20 min. The mix was centrifuged at 15,000 rpm for 30 min and the supernatant was transferred into a new tube. 500 μl supernatant sample was used as input. All experiments were performed on ice. Anti-c-Myc Magnetic Beads (Sigma-Aldrich) were washed using 600 mL NT2 buffer (50 mM HEPES pH 7.5, 0.05% NP-40, 200 mM NaCl, 0.5 mM DTT, 2 mM EDTA, 40 units/mL RNase Inhibitor, and 1× cocktail). The supernatants were incubated with the washed Anti-c-Myc Magnetic Beads for 4 h, and the complexes were collected with a magnet and washed 5 times using NT2 buffer.

Protease K digestion

The complexes were resuspended in 150 μl of protease buffer (75 mM NaCl, 50 mM Tris-HCl pH = 7.5, 1% [w/v] SDS, 6 mM EDTA) before 2 mg/mL of proteinase K was added, and the samples were incubated for 30 min at 50°C. The eluted beads were removed with a magnet. Homogenization buffer (100 mM Tris–HCl pH = 8.0, 100 mM NaCl, 0.5% SDS, 5 mM EDTA and 1% β-mercaptoethanol) was added to the supernatant to 500 μl and the samples were mixed well.

RNA recovery and quantitative PCR

The RNA were recovered and used for library generation with the SMARTer Stranded Total RNA-Seq Kit (Takara). Sequencing was performed on an Illumina HiSeq4000 in single-read mode with 50 bp per read. The clean reads were aligned to the cucumber genome using STAR (version 2.6.0cr).[48] The enriched regions (peaks) in each IP sample were detected by MACS2 (version 2.1.1.20160309)[49] with $q < 0.01$ and the corresponding input sample was used as the control. The RNA was also recovered and reverse transcribed to cDNA using the M-MLV Reverse Transcriptase (Promega). The relative fold enrichment was determined by qPCR. *CsNADH*, *Csa-V3_UNG208130*, was used as the control. The primers used for FA-CLIP-qPCR are listed in Table S2. The processed sequencing data were summarized in Table S3.

m^{6}A-seq and m^{6}A-RIP-qPCR

Total RNA was extracted using TRIzol from the ovaries of *YTH1*^{W} *ACS2*^{W} and *YTH1*^{W} *ACS2*^{C} *in planta* and the cotyledons of cucumber in the transient expression system. Two biological replicates were used for m^{6}A-seq, and five ovaries from five independent plants were pooled as one biological replicate for stable transgenic plants. Three biological replicates were used for m^{6}A-RIP-qPCR, and five infiltrated cotyledons from five independent plants were sampled as one biological replicate for cucumber cotyledons in the transient expression system. The mRNA was isolated with the PolyA Ttract® mRNA Isolation System (Promega). 5 μg mRNA was incubated with Protein A Dynabeads (Thermo) at 4°C for 2 hours to remove non-specifically bound RNA. 5 μg m^{6}A antibody (Synaptic Systems) was used for immunoprecipitation in IP buffer (50 mM Tris–HCl pH = 7.4, 300 mM NaCl, 0.5% Igepal CA-630, 2 mM RVC (Sigma-Aldrich) and 0.5mg/mL BSA) at 4°C for 3 hours. The enriched mRNA was eluted with m^{6}A buffer (1 × IP buffer and 6.7 mM N^6-Methyladenosine,5'-monophosphate sodium salt). Both m^{6}A-IP mRNA and input mRNA were recovered and used for library generation with the SMARTer Stranded Total RNA-Seq Kit (Takara). Sequencing was performed on an Illumina HiSeq4000 in single-read mode with 50 bp per read. Sequencing reads were aligned to the cucumber genome using STAR (version 2.6.0cr).[48] The m^{6}A-enriched regions (peaks) in each m^{6}A-IP sample were detected by MACS2 (version 2.1.1.20160309)[49] with $q < 0.01$ and the corresponding m^{6}A-input sample was used as the control. Peaks that were detected in both replicates were considered high-confidence peaks. The peak annotation and binding motifs were analyzed by HOMER (version 4.9).[50] The recovered m^{6}A-IP mRNA and input mRNA were also used to calculate fold enrichment using qPCR. *CsNADH* was used as the control gene. The primers used are listed in Table S2. The processed sequencing data were summarized in Table S4.

eTAM seq and site-specification amplification

The eTAM seq technique was carried out to detect the m^{6}A methylation on *ACS2* at single base resolution as previously described (eTAM).[27] In summary, the purified mRNA (300 ng) from stable transgenic materials (*WW* and *WC*) were depleted of poly(A) tails, end-repaired, ligated to 3′-adapters and immobilized on Dynabeads MyOne Streptavidin C1 (Invitrogen). RNA samples were deaminated twice on beads for 3h at 37°C using 200 pmol of TadA8.20 in the deamination buffer. The beads were washed and eluted by boiling them in DNase-free water (Invitrogen) and immediately transferring them into new tubes. The eTAM seq libraries were constructed using the NEBNext® Multiple Small RNA Library Prep Set for Illumina® (catalog no. E7300S) and sequenced on an Illumina HiSeqTM X10. Sites of interest were PCR amplified from the eluted cDNA using transcript-specific primers (listed in Table S2), which were designed to recognize sequences post-deamination, including sequences surrounding the target m^{6}A sites. The PCR fragments were sequenced on an Illumina MiSeq instrument.

ALKBH10B-associated SELECT for detection of m^{6}A

The ALKBH10B-associated SELECT assay was used to detect the m^{6}A methylation on adenosine around *ACS2* 1287 synonymous mutation as previously reported.[28] The total RNA was extracted from the infiltrated cotyledons using Trizol reagent (Invitrogen) and

the mRNA was isolated using the PolyATtract® mRNA Isolation System (Promega). Five infiltrated cotyledons from independent plants were sampled as one biological replicate, and three biological replicates were used for analysis. 100 μL reaction mix containing 2 μg mRNA,12 μg ALKBH10B protein, which had been expressed using the TNT® SP6 high-yield wheat germ expression system (Promega), 2 mM L-ascorbic acid (Sigma, A92902), 300 μM α-KG (Apexbio, M1277-50), 283 μM $(NH_4)_2Fe(SO_4)_2$ (Sigma, 203505), 50 mM HEPES (pH=7.0), and 0.2 U/μl RNase inhibitor (Thermo Fisher, EO0381) was incubated at 37°C for 30 minutes and inactivated at 95°C for 5 minutes. The reaction was stopped by adding 20 mM EDTA. As the control (ALKBH10B-EDTA), 20 mM EDTA was added before the demethylation reaction. RNA was recovered and quantified using Qubit 4 (Thermo) with a Qubit™ RNA HS Assay Kit (Thermo, Q32852). Then, 5 μg demethylated mRNA was mixed with 40 nM Up and Down Primer and 5 μM dNTP in 17 μl 1 × CutSmart buffer (NEB, B6004). The reaction mix was annealed in a Thermal Cycler. Next, 0.01 U *Bst* 2.0 DNA polymerase (NEB), 0.5 U SplintR ligase (NEB) and 10 nmol ATP were added to the 17 μl annealing products and samples were incubated at 40°C for 20 min, then 80°C for 20 min. qPCR experiments were performed using the qPCRF and qPCRR primers on a CFX Connect Real-Time System (Bio-Rad) using GoTaq® qPCR Master Mix (Promega). The primers used are listed in Table S2.

Absolute quantification of m^{6}A modification

To detect the absolute m^{6}A levels on A^{1286} of *ACS2* mRNA, the left probe and right probe with PCR adapters complementary anneal to target-specific sequence and leave a base gap at target site were designed. m^{6}A marks could serve to selectively hinder the activity of T3 DNA ligase, resulting in a significant reduction of the production of ligation fragments from m^{6}A-containing RNA compared with that from unmodified RNA. The total RNA was isolated from infiltrated cotyledons of *ACS2*^{1287C} and *ACS2*^{1287T}, materials treated with ALKBH10B were used as control. The ligation reaction mix A containing 20 nM left and right probe, 100 ng RNA and 1 × T3 ligation buffer was incubated at 85°C for 3 min and 35°C for 10 min. T3 ligase with an appropriate amount and ligation buffer was added to Mix A to final volume of 20 μL and then was incubated at room temperature for 10 min and used for subsequent real-time qPCR. The schematic diagram was shown in Figure S4S. The Probes and primers used are listed in Table S2.

Ribosome profiling

Cucumber ovaries from *WW*, *KW*, *WC*, and *KC* were treated with 100 μg/ml cycloheximide (Sigma) to block translational elongation. Ten fruits from different plants were sampled as one biological replicate, and two biological replicates were used for analysis. The samples were immediately frozen in liquid nitrogen and ground to a powder. The ribosomal profiling technique was performed as previously reported, with some modifications.[59] Resuspended extracts in lysis buffer were transferred to new microtubes, mixed with a pipette several times and incubated on ice for 10 min. Lysates were then triturated ten times through a 26-G needle before centrifugation at 20,000 g for 10 min at 4°C. To prepare RNA fragments (RFs), 1 μL RNase I and 6 μL of DNase I were added to the lysate (400 μL), which was then incubated for 45 min at room temperature with gentle mixing. The nuclease digestion was stopped by the addition of the SUPERase·In RNase inhibitor (10 μL). Size exclusion columns (GE Healthcare; catalog no. 27-5140-01) were equilibrated with polysome buffer (3 mL) by gravity flow and centrifuged at 600 g for 4 min. Digested RFs (100 μL) were added to the column and centrifuged at 600 g for 2 min. Next, 10 μL 10% (w/v) SDS was added to the elution, and RFs larger than 17 nt were isolated using the RNA Clean and Concentrator-25 kit (Zymo Research; R1017). RFs without rRNA were further purified using magnetic beads (Vazyme, Nanjing, Jiangsu, China). Ribo-seq libraries were constructed using the NEBNext® Multiple Small RNA Library Prep Set for Illumina® (catalog no. E7300S) and sequenced on an Illumina HiSeqTM X10 by the Gene Denovo Biotechnology Co. (Guangzhou, China). The low quality reads were filtered by fastq and adapter sequences were trimmed. The reads were mapped to ribosome RNA (rRNA) database, GeneBank, Rfam database were removed using short reads alignment tool Bowtie2. Processed RNA reads were mapped to the cucumber genome by STAR[48] with 2-pass setting enabled. SAMtools[51] were used to select the reads which mapped uniquely reads. The number of reads in the coding regions were counted using HOMER (version 4.9).[50] The translational efficiency (TE)[60] was defined as: TE = Norm data in Ribo-seq/Norm data in RNA-seq. The processed sequencing data were summarized in Table S5.

Ethylene release measurement

Ethylene production was quantified using the 0 DAA fruits from *WW*, *KW*, *WC*, and *KC*. Three fruits from different plants were sampled as one biological replicate and three biological replicates were used for analysis. Each fruit was excised and placed in a 10 ml glass flask containing a piece of wet cotton and MS liquid medium. The flask was sealed with a rubber cap to prevent ethylene leakage, and the flask was left at 23°C for 1 hour before the container was opened, and the gas was replaced with N_2 to exhaust the ethylene induced by wounding. The fruits were incubated in flasks at 23°C for 10 h to accumulate ethylene, and 10 μL of gas was harvested with a syringe and injected into the gas chromatograph (Agilent 7890B-5977A). All measurements were repeated three times. The ethylene release rate was defined as nL g^{-1} FW h^{-1} (the volume of ethylene released per hour per gram of fruit).

RNA electrophoretic mobility shift

The recombinant His-YTH1 proteins were expressed and purified from *E. coli* BL21 (DE3). Biotinylated RNA probes were synthesized with or without m^{6}A modification in Sangon Biotech Co., Ltd. (Shanghai, China). To determine the binding affinity of YTH1 for the RNA probes with or without m^{6}A modification, EMSA assays were performed using LightShift Chemiluminescent RNA EMSA Kit (Thermo Scientific, 20158). The experiment was carried out following the manufacturer's protocol, the recombinant protein His-YTH1 was

Please cite this article in press as: Xin et al., Recessive epistasis of a synonymous mutation confers cucumber domestication through epi-transcriptomic regulation, Cell (2025), https://doi.org/10.1016/j.cell.2025.06.007

diluted to gradient concentration (0 nM, 200 nM, 1 μM and 5 μM) and incubated with 1 μl of RNA probes (4 nM) for 30 min at room temperature. The protein–RNA complexes were loaded onto the polyacrylamide gel for 90 min at 90 V. Then the complexes were transferred to nylon membranes and crosslinked using UV-light (254 nm, 40-60s). Finally, the Biotin-labeled RNA were detected by chemiluminescence. The Biotin-labeled RNA probe are listed in Table S2.

In vivo smStructure-seq library construction

Dimethyl sulphate (DMS) was used to obtain the *in vivo* smStructure-seq library. In brief, 7-day-old cucumber seedlings were infiltrated with agrobacteria carrying constructs, leaves were harvested 4 days after infiltration, submerged in 15 ml 1× DMS reaction buffer (200 mM potassium acetate, 200 mM Bicine (pH 8.0) and 5 mM $MgCl_2$) in a 50-ml Falcon tube. 1% DMS was used to treat the leaves for 15 min at 30°C with 800 rpm shaking. After quenching the reaction with freshly prepared dithiothreitol (DTT), the samples were washed with deionized water and immediately frozen with liquid nitrogen and ground into powder. Total RNA was extracted using Qiagen RNeasy kit, followed by DNase I treatment following the manufacturer's protocol. The control group was prepared using water (labeled as minus), following the same procedure described above. Reverse transcription was done by Induro® Reverse Transcriptase with 5 × RT buffer (250 mM Tris–HCl pH 8.3, 375 mM KCl, 25 mM DTT, 7.5 mM $MnCl_2$) and 1 μl RNase inhibitor. The whole reaction system in the tube was incubated at 60°C for 120 min. To remove the Induro enzyme from the template, 1 μl Proteinase K was used after RT reaction. PCR reactions with 15 cycles were done with specific primers (Table S2) using KOD Xtreme Hot Start DNA Polymerase (Novagen). Two independent biological replicates were generated for both plus and minus smStructure-seq libraries. The purified DNA samples were subjected to Nanopore library construction by following the manufacturer's instructions of the native barcoding kit (NBD-24).

smStructure-seq data analysis

Raw reads from both plus and minus samples were basecalled and demultiplexed using Dorado (https://github.com/nanoporetech/dorado). The resulting reads were mapped using minimap2[54] with the following parameters: minimap2 -t 8 -ax splice –secondary=no -G 12000. Reactivity was then calculated using the RNA Framework pipeline.

To generate the overall DMS reactivity profiles, the mutation rate at each nucleotide was calculated by dividing the number of mutations by the number of reads at that location. The raw reactivity for a given nucleotide was then calculated as the difference between the rescaled plus and minus samples. To facilitate comparison, the raw reactivity was normalized to a standard scale ranging from 0 (indicating no reactivity) to approximately 1 (indicating high SHAPE reactivity), reflecting the mutational profiles. Box-plot normalization[61] was applied to further normalize the raw reactivity.

Calculation of ΔG_{unfold}

The energy required for each translocation step (ΔG_{unfold}) was estimated using the following approach:[37]

$$\Delta G_{unfold} = \Delta G_{cons} - \Delta G_{ref}$$

ΔG_{ref} represents the free energy of the SHAPE-directed transcript structure, while ΔG_{cons} denotes the free energy of the "constrained" transcript structure, in which each sliding window is constrained to remain single-stranded. All free energy calculations were performed using the eval function of the ViennaRNA package,[52] excluding SHAPE pseudo-energy contributions. Finally, the energy difference between the 1287C and 1287T alleles ($\Delta\Delta G$) was calculated to assess the impact of the mutation.

Structural analysis by DaVinci

The whole pipeline of DaVinci was performed as previously described with few modifications.[33] Briefly, the single-stranded constraints were incorporated into the SCFG engine within the DaVinci pipeline. RNA structures, constrained by individual bit vectors, were generated and collected. To reduce the background noise, any positions where the mutation rate in the minus sample was equal to or greater than that in the positive sample were excluded as constraints in the CONTRAfold folding step.[62] Since different structures could exhibit identical mutational profiles during probing. These RNA structures were then converted into dot-bracket notation, followed by transformation into RNA structural elements using the rnaConvert function from the Forgi package.[53] The digital RNA secondary structure elements were extracted, forming a numeric matrix that was subjected to dimensionality reduction techniques such as PCA. Clustering was performed on the dimensionality reduction output using k-means, with the value of k determined visually, employing the k-means function from scikit-learn. The representative structure for each cluster was identified by calculating the most prevalent RNA structure type at each position, representing the maximum expected accuracy, and choosing the RNA structure closest to the center of the cluster that best matches the most common structure. Base-pair probabilities were computed by determining the frequency of each base-pair in the conformation space. Positional base-pair probabilities were calculated as:

$$P_i = \sum_{j}^{J} P_{ij}$$

P_{ij} represents the probability of base i pairing with base j across all potential pairing partners. The likelihood of single-strandedness was derived using $1 - P_{ij}$.

Please cite this article in press as: Xin et al., Recessive epistasis of a synonymous mutation confers cucumber domestication through epi-transcriptomic regulation, Cell (2025), https://doi.org/10.1016/j.cell.2025.06.007

QUANTIFICATION AND STATISTICAL ANALYSIS

Sample numbers (n) and statistical analysis are detailed in each method's section above, and indicated in each figure legend. Statistical analysis was performed with GraphPad Prism 10 (https://www.graphpad.com). Results are represented as mean ± standard deviation. One-way ANOVA and Student's t-test were used to obtain p values and different letters above bars represent the significant difference at $p < 0.05$. p values are indicated above each bar graph.

CellPress
OPEN ACCESS

Supplemental figures

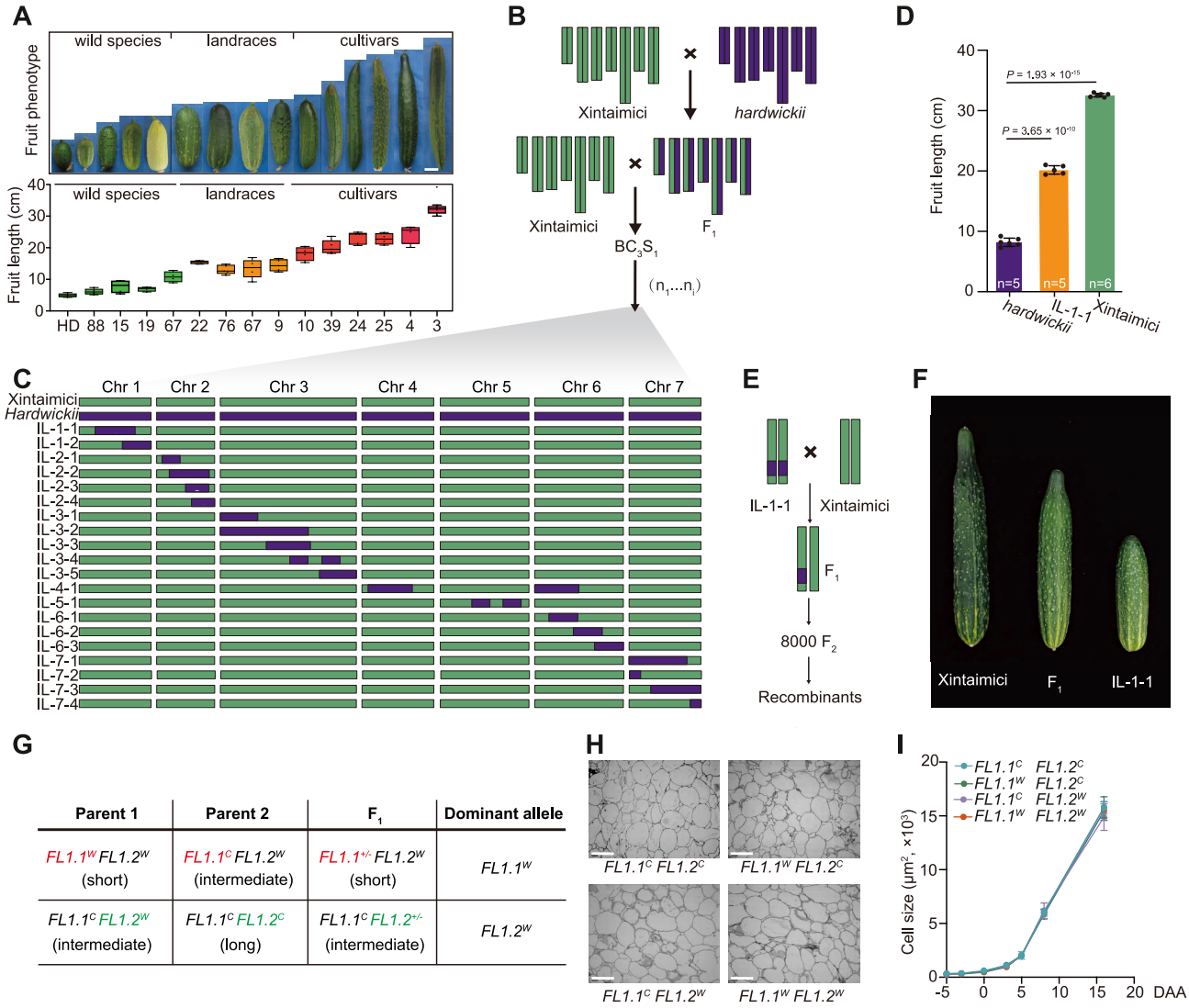

Parent 1	Parent 2	F_1	Dominant allele
FL1.1^W *FL1.2*^{W} (short)	*FL1.1*^{C} *FL1.2*^{W} (intermediate)	*FL1.1*$^{+/-}$ *FL1.2*^{W} (short)	*FL1.1*^{W}
FL1.1^C *FL1.2*^{W} (intermediate)	*FL1.1*^{C} *FL1.2*^{C} (long)	*FL1.1*^{C} *FL1.2*$^{+/-}$ (intermediate)	*FL1.2*^{W}

Figure S1. Identification of the *FL1.1* QTL for fruit length domestication, related to Figure 1

(A) The fruit length of wild species and cultivated cultivars. Upper: phenotype, scale bar, 5 cm; lower: length of fruits. Data are means ± SD. *n* = 3 fruits from different plants.

(B) Construction process of the backcrossed IL population. Xintaimici (green) and *hardwickii* (purple) were used as the parental lines. The F_1 population derived from the crossing of the parental lines resulted in a heterozygous genotype on all chromosomes. By crossing F_1 with Xintaimici three times, a BC_3S_1 population with segregating genotypes was produced. The final ILs were generated by self-crossing BC_3S_1 4–6 times.

(C) The bin-map of 20 ILs. Purple, *hardwickii* genotype; green, Xintaimici genotype.

(D) Fruit length of *hardwickii*, Xintaimici, and IL-1-1. Data are means ± SD. *n*, number of fruits from different plants. Statistical significance was determined using two-tailed Student's t tests.

(E) Diagram showing the production of 8,000 F_2 recombinants using IL-1-1 and Xintaimici.

(F) Representative fruit of the F_1 progeny from the cross between Xintaimici and IL-1-1. Scale bar, 5 cm. F_2 segregation pattern fitted a Mendelian ratio of 1:2:1 (F_2 population of 103 individuals, 28 long fruits, 53 intermediate-length fruits, and 22 short fruits, $\chi^2 = 0.786$, $p = 0.675$).

(G) Genetic analysis of *FL1.1* and *FL1.2* in F_1 generated by crossing the different parents.

(H) Longitudinal sections of the fruit mesocarp in four genotypes at 16 days after anthesis (DAA). Scale bars, 200 μm.

(I) The average cell size in the mesocarp along the longitudinal axis shows no significant difference among the four genotypes. Data are means ± SD. *n* = 3.

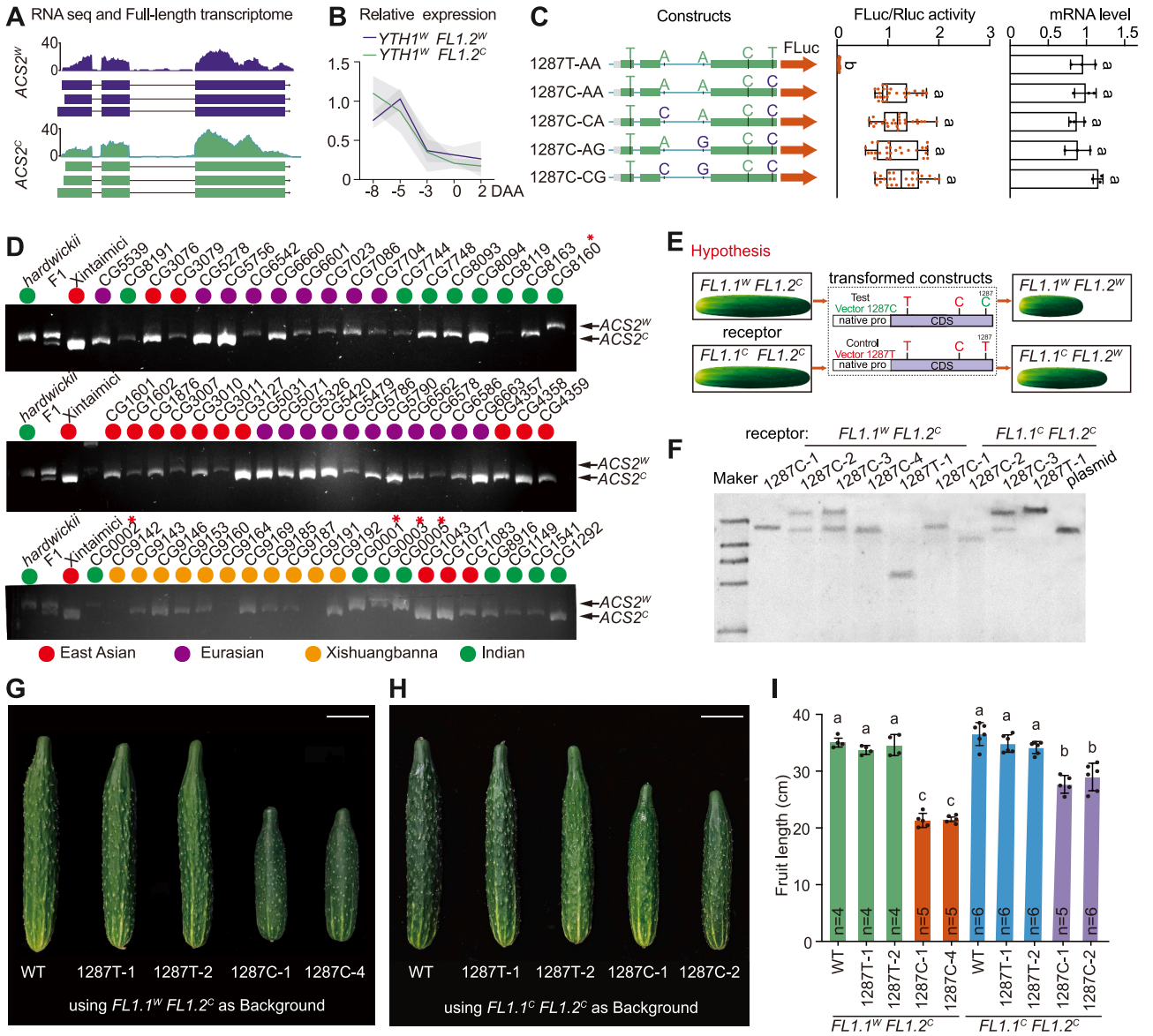

Figure S2. Detection of the *ACS2* variants in 115 core cucumber collections and genetic validation of *ACS2*, related to Figure 2

(A) Full-length transcriptome and RNA-seq reads showed that the SNPs of *ACS2* did not cause differences in splicing and expression.

(B) The *ACS2* gene shows similar expression levels and patterns during early fruit development between the *FL1.1*^{W} *FL1.2*^{W} and *FL1.1*^{W} *FL1.2*^{C} genotypes. Data are means from three independent fruits ± SD. Colored lines indicate median expression, with gray areas representing the 5th and 95th quantiles.

(C) Functional identification of the SNPs on the intron using dual-luciferase reporter assays. Left, schematic showing all constructs used. Green and purple letters represent the *ACS2*^{C} and *ACS2*^{W} genotypes SNP, respectively. Middle: FLuc/RLuc activities of the corresponding constructs are shown on the left. Data are means ± SD (n = 16). Different letters indicate significant differences (p < 0.05, one-way ANOVA and Tukey's test). Right, relative *ACS2* mRNA expression levels from the corresponding constructs. Data are means ± SD (n = 3).

(D) Detection of the *ACS2* variants in core cucumber collection by derived cleaved amplified polymorphic sequences (dCAPS) makers. The PCR fragment amplified from *ACS2*^{C} is smaller than that from *ACS2*^{W} after being treated with *Bsa*BI restriction endonuclease. Dots of different colors represent cucumbers from different groups. The stars in red indicate the cucumber germplasm with *ACS2*^{W} alleles.

(E) Hypothetical diagram for verifying the function of *ACS2*^{W} by transferring vector 1287C to *FL1.1*^{W} *FL1.2*^{C} and *FL1.1*^{C} *FL1.2*^{C}. The dotted boxes indicate the two vectors with only one synonymous mutation.

(F) Detection of transformed genetic transformation materials by Southern blot.

(G and H) Plants stably transformed with the 1287C construct had significantly shorter fruit than plants transformed with the 1287T construct or wild type (WT), at 16 DAA. Scale bar, 5 cm.

(I) Quantification of fruit length related to (G) and (H). Data are means ± SD. n, number of fruits from different plants. Different letters indicate significant differences (p < 0.05, one-way ANOVA and Tukey's test).

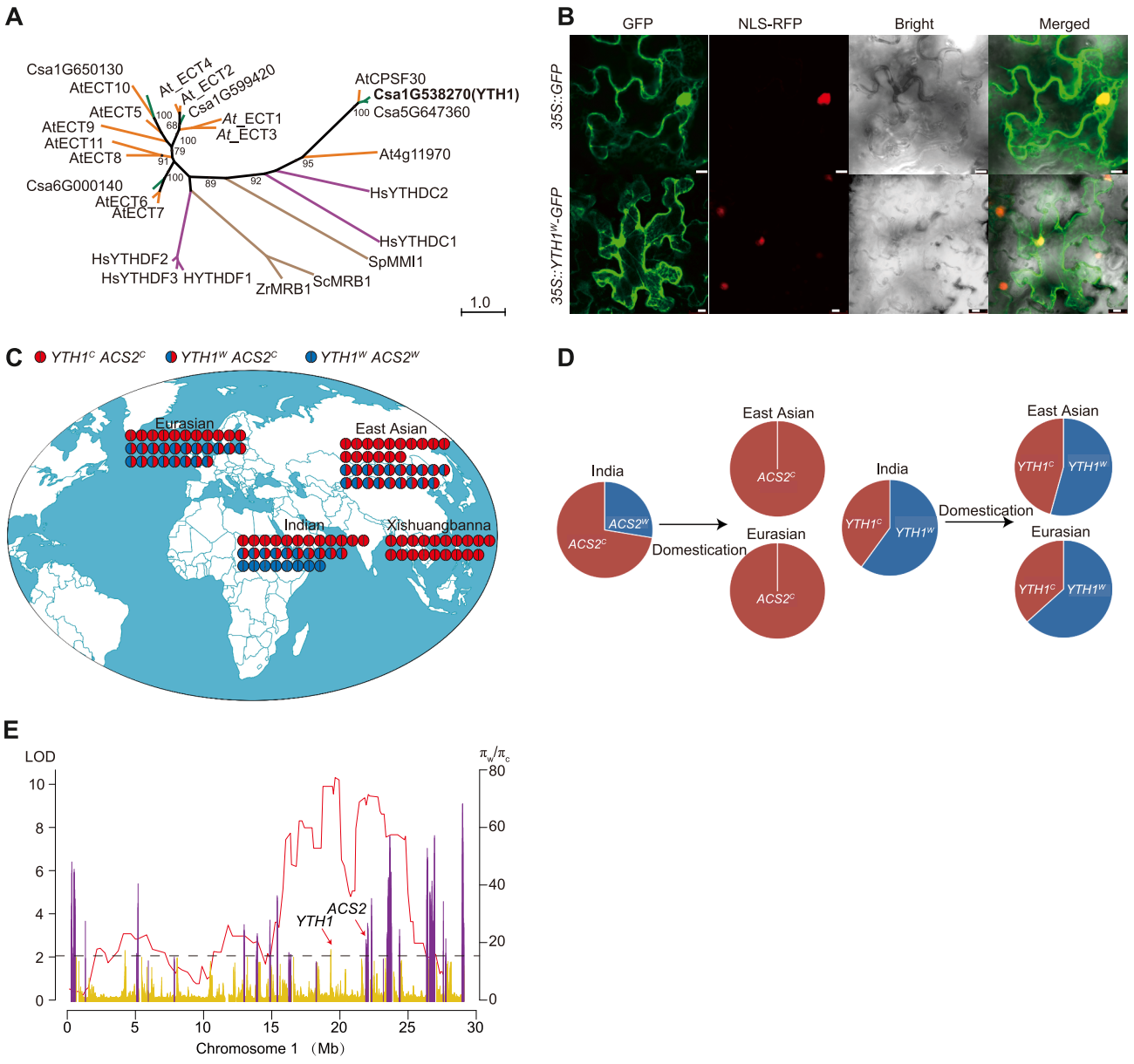

Figure S3. Characterization of the *YTH1* gene, related to Figure 3

(A) Phylogenetic relationship of YTH domain proteins in cucumber (green), *Arabidopsis thaliana* (orange), human (magenta), and three yeast YTH domain proteins (brown). The length of the branches represents the evolutionary distance.

(B) Subcellular localization of *35S::GFP* and *35S::YTH1^W-GFP* in *Nicotiana benthamiana* leaf epidermal cells. NLS-RFP, RFP fluorescence of the nuclear localization signal; Bright, bright field; Merge, merged image of GFP, NLS-RFP, and bright-field images. Scale bars, 10 μm.

(C and D) The distribution of *YTH1* and *ACS2* alleles in a cucumber population. The results revealed that the *ACS2^C* allele was subject to strong selection in cultivated cucumber (Eurasian and East Asian types) during domestication, while the *YTH1^W* and *YTH1^C* alleles were evenly distributed among the population. Color codes indicate the genotype. Red and blue, cultivar and wild, respectively.

(E) Selective sweep result showing that *ACS2* is present in the sweep region. The purple bars indicate candidate sweeps, and gold bars represent windows that are not considered to be candidate sweeps.

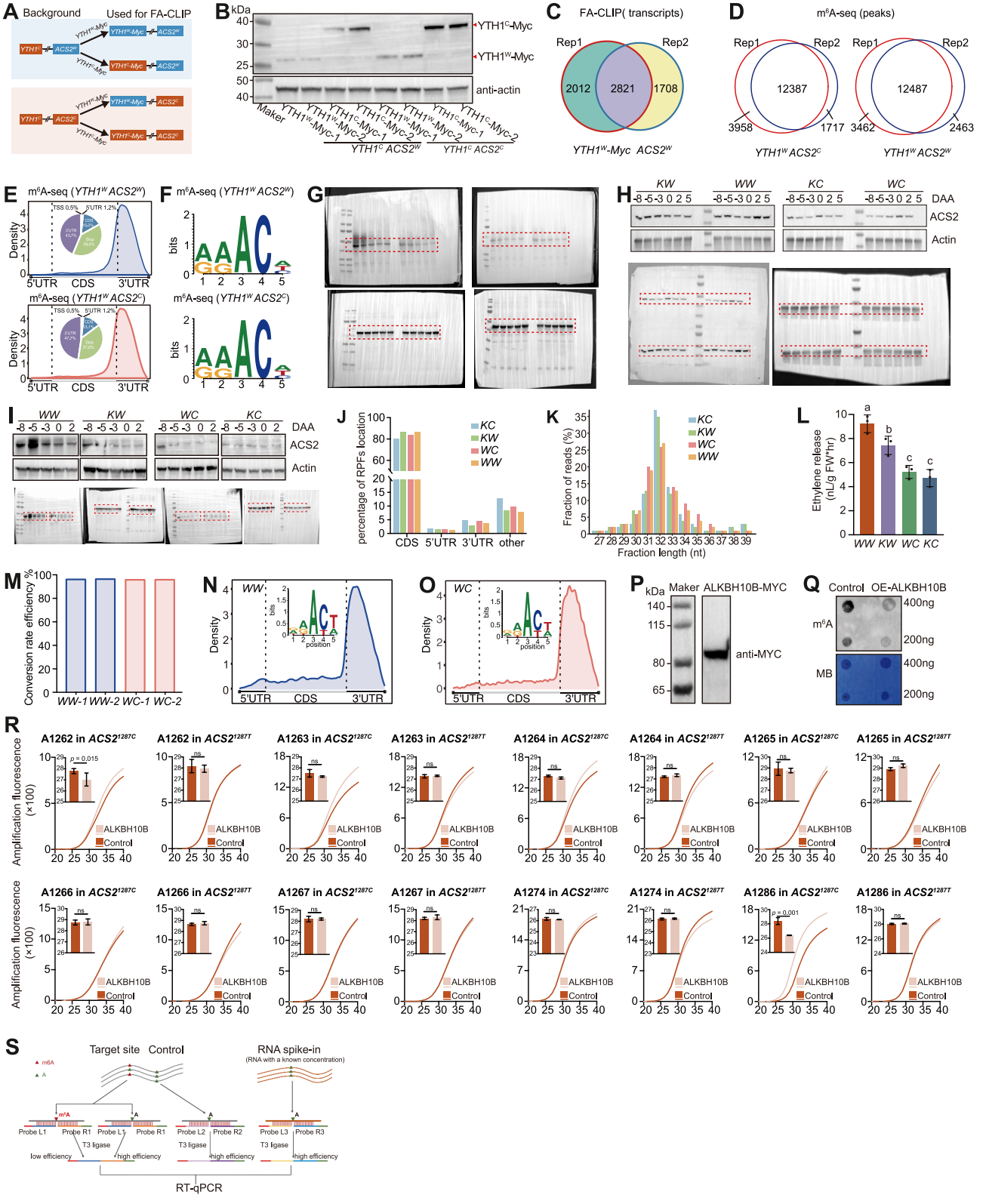

(legend on next page)

Figure S4. Detection of m^{6}A methylation at A^{1286} of the ACS2 mRNA, related to Figure 4

(A) The production process of materials used to perform FA-CLIP experiments.

(B) Detection of protein expression of *YTH1^W-Myc* and *YTH1^C-Myc* in transgenic materials by immunoblotting analysis using anti-Myc antibody. Actin was detected as internal control.

(C) Overlap of YTH1-binding transcripts from FA-CLIP of two biological replicates in *YTH1^W-Myc ACS2^W*.

(D) Overlap of m^{6}A methylated peaks from m^{6}A-seq of two biological replicates in *YTH1^W ACS2^W* and *YTH1^W ACS2^C*.

(E) Metagene profiles showing the m^{6}A site, which was identified by m^{6}A-seq, distribution across transcripts in *YTH1^W ACS2^W* and *YTH1^W ACS2^C*. The transcript is segmented into three regions: 5′ UTR, CDS, and 3′ UTR. The percentage (%) of overall m^{6}A sites distributed in 5′ UTR, CDS, and 3′ UTR regions was shown in a pie chart.

(F) The conserved sequence motif for m^{6}A-containing peak regions.

(G–I) Uncropped immunoblotting images of three replicates, related to Figure 4F.

(J) Percentage of ribosome footprints' (RPFs) location in CDS, 5′ UTR, 3′ UTR, and others for four materials.

(K) Percentage distribution of RPFs length.

(L) Ethylene production in the four genotypes (*WW*, *KW*, *WC*, and *KC*). Data are means ± SD. $n = 3$ independent biological replicates. Different letters indicate significant differences ($p < 0.05$, one-way ANOVA and Tukey's test).

(M) Transcriptome-wide A-to-G conversion efficiency of eTAM-seq in two independent replicates.

(N and O) Metagene profiles showing the m^{6}A site, which was identified by eTAM-seq, distribution across transcripts in *WW* and *WC*. The consensus sequence hosting m^{6}A is inserted.

(P) Immunoblotting analysis using anti-MYC antibody showing the expression of ALKBH10B-MYC.

(Q) Overexpression of the cucumber homologs of the m^{6}A demethylase gene, *ALKBH10B*, can significantly reduce the global m^{6}A level in cucumber cotyledons. Methyl blue (MB) staining shows identical loading of total RNA.

(R) SELECT results for detecting m^{6}A modification at all the adenosine around the 1287 synonymous mutation in *ACS2^{1287C}* and *ACS2^{1287T}*. The m^{6}A demethylase ALKBH10B-MYC was used in this assay to eliminate the m^{6}A modification. Data are mean ± SD. $n = 3$. Two-tailed Student's t tests.

(S) Schematic representation of experiment for absolute quantification of m^{6}A modification.

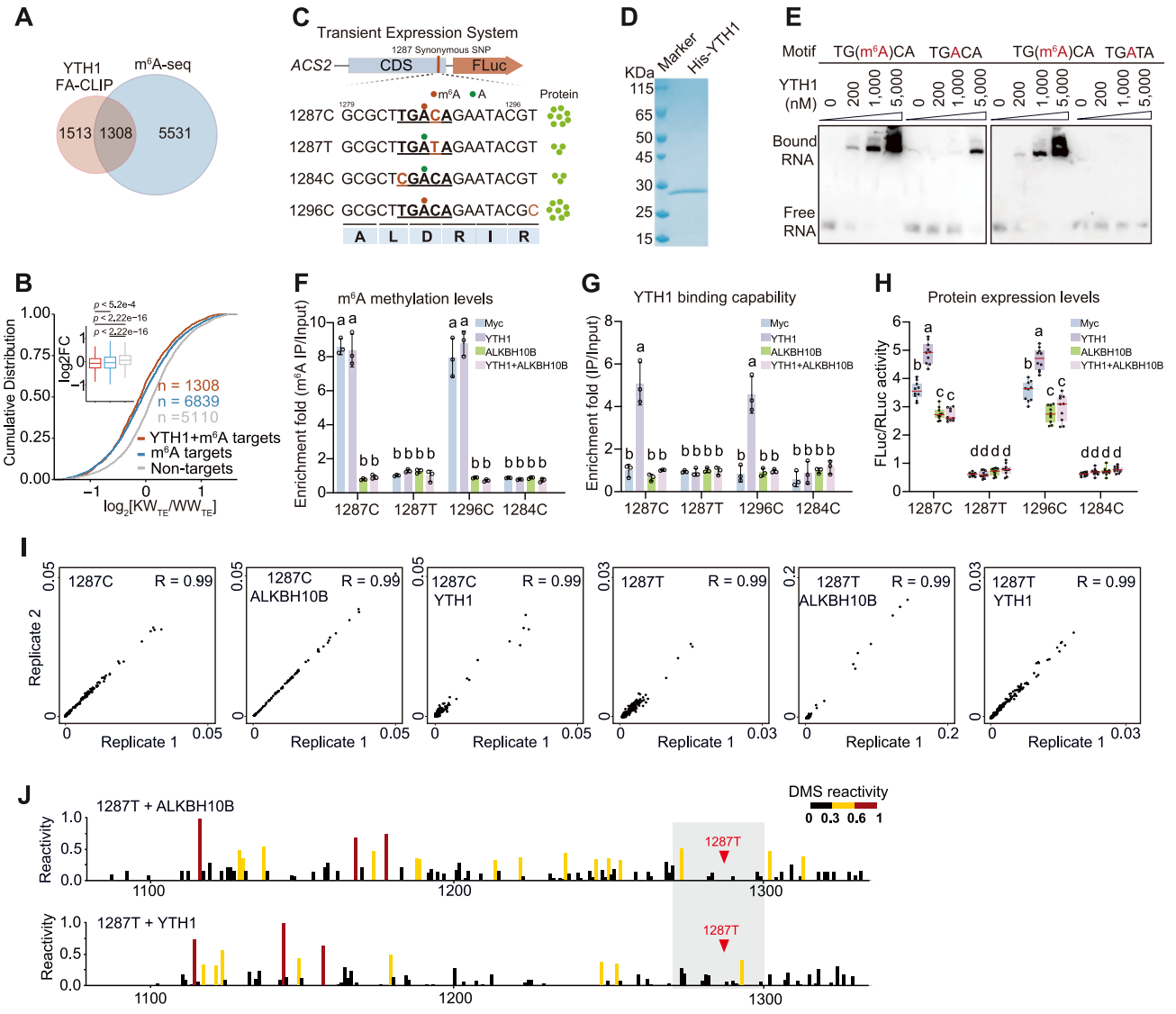

Figure S5. m^{6}A modification and mRNA structural conformation together determine the protein TE of ACS2, related to Figure 5

(A) Overlap of target genes identified by m^{6}A-seq and FA-CLIP.

(B) Cumulative distribution of the fold change in translational efficiency between *WW* (WW_{TE}) and *KW* (KW_{TE}). *p* values were calculated using a two-sided Student's t test; *n* = 2 independent biological replicates for ribosome profiling. Box-plot elements: center line, median; box limits, upper and lower quartiles; whiskers, 1%–99%.

(C) Synonymous mutation constructs 1284C and 1296C, changing T^{1284} and T^{1296} into C on the basis of 1287C. The letters in red represent the mutated site. The DRACH motif is highlighted in bold. The number of green dots represents the protein production.

(D) Coomassie blue staining showing the recombinant protein His-YTH1 purified from *E. coli*.

(E) Gel-shift assay also revealed that YTH1 has a higher binding affinity to the methylated $ACS2^{1287C}$ probe compared with the unmethylated $ACS2^{1287T}$ probe, as well as a slight preference for the unmethylated $ACS2^{1287C}$ probe. The *ACS2* 1287 C>T synonymous mutation completely eliminated the affinity of YTH1 to $ACS2^{1287T}$.

(F–H) Transient expression assays show that $YTH1^W$ binds to the m^{6}A modification and increases the protein levels of $ACS2^{1287C}$ and $ACS2^{1296C}$, which can also be blocked by treatment with ALKBH10B. (F) m^{6}A-RIP-qPCR showed the m^{6}A methylation level of $ACS2^{1287C}$ and $ACS2^{1287T}$ co-expressed with Myc, YTH1-Myc, and ALKBH10B-Myc, respectively. Data are means ± SD. Different letters indicate significant differences ($p < 0.05$, one-way ANOVA and Tukey's test; $n = 3$). (G) FA-CLIP showed the capability of $YTH1^W$ binding to $ACS2^{1287C}$ and $ACS2^{1287T}$ co-expressed with Myc, YTH1-Myc, and ALKBH10B-Myc, respectively. Data are means ± SD. Different letters indicate significant differences ($p < 0.05$, one-way ANOVA and Tukey's test; $n = 3$). (H) Dual-luciferase reporter assays showed the protein expression level of $ACS2^{1287C}$ and $ACS2^{1287T}$ co-expressed with Myc, YTH1-Myc, and ALKBH10B-Myc, respectively. Data are means ± SD. Different letters indicate significant differences ($p < 0.05$, one-way ANOVA and Tukey's test; $n = 20$).

(legend continued on next page)

(I) Scatter plot of raw reactivities across two biological replicates for the DMS-treated samples of *ACS2*^{1287C}, *ACS2*^{1287C} co-expressed with *ALKBH10B*, *ACS2*^{1287C} co-expressed with *YTH1*, and 1287T, respectively.
(J) DMS reactivity profile of the *ACS2* alleles. Bar plots showing the DMS reactivity of the indicated region on the *ACS2* locus for the *ACS2*^{1287T}, *ACS2*^{1287C}, and *ACS2*^{1287C} co-expressed with *ALKBH10B* and *YTH1*, respectively. Red triangles show the position of the 1287 synonymous mutations.